Comput Visual Sci (2009) 12:267–285
DOI 10.1007/s00791-008-0113-1

REGULAR ARTICLE

Image segmentation using a multilayer level-set approach

Ginmo Chung · Luminita A. Vese

Received: 31 January 2007 / Accepted: 29 August 2007 / Published online: 10 April 2008

Abstract We propose an efficient multilayer segmentation method based on implicit curve evolution and on variational approach. The proposed formulation uses the minimal partition problem as formulated by D. Mumford and J. Shah, and can be seen as a more efficient extension of the segmentation models previously proposed in Chan and Vese (Scale-Space Theories in Computer Vision, Lecture Notes in Computer Science, Vol. 1682, pp. 141–151, 1999, IEEE Trans Image Process 10(2):266–277, 2001), and Vese and Chan (Int J Comput Vis 50(3):271–293, 2002). The set of unknown discontinuities is represented implicitly by several nested level lines of the same function, as inspired from prior work on island dynamics for epitaxial growth (Caflisch et al. in Appl Math Lett 12(4):13, 1999; Chen et al. in J Comput Phys 167:475, 2001). We present the Euler–Lagrange equations of the proposed minimizations together with theoretical results of energy decrease, existence of minimizers and approximations. We also discuss the choice of the curve regularization and conclude with several experimental results and comparisons for piecewise-constant segmentation of gray-level and color images.

1 Introduction

This work is devoted to the problem of piecewise-constant segmentation of images using functional minimization, Euler–Lagrange equations, and implicit representation of the discontinuity set. The proposed formulation can also be seen as a free boundary problem or as a shape optimization problem. Assuming a degradation model of the form $f(x) = \sum_i c_i \chi_{\Omega_i}(x) + noise$, we seek to recover optimal partitions with constants c_i and regions Ω_i. Here Ω is an open, bounded and connected domain with Lipschitz boundary, and $f : \Omega \to \mathbb{R}$ is a given observed image. As in the minimal partition problem of Mumford and Shah [18], we assume that $f \approx c_i$ within each Ω_i, and that the open regions Ω_i, together with their boundaries, make-up Ω. Thus, this work is in the spirit of the minimal partition problem [18] and its implicit formulation as introduced in [5,6,27] (under the assumption of an upper bound on the number of segments), using the variational level-set approach [29]. However, the unknown set of curves Γ making up the set of discontinuities is represented here using a nested structure of level lines of the same implicit function. In the standard front propagation approach [11,12,19], only the zero level line of the same function ϕ is used to represent free boundaries. Borrowing the idea from prior work on island dynamics for epitaxial growth [2,7,14], the proposed methods thus lead to more efficient multi-phase implicit representations. We first give the main ingredients used in our approach.

The minimal partition problem In order to obtain an optimal piecewise-constant approximation of a given image-data f, Mumford and Shah [18] proposed the following: given a function f in $L^\infty(\Omega)$ (induced by the L^2-topology), find a set of disjoint open regions Ω_i, such that $u = c_i$ in each Ω_i is a minimizer of [18]

$$F(u, \Gamma) = \sum_i \int_{\Omega_i} |f - c_i|^2 dx + \mu \mathcal{H}^{n-1}(\Gamma), \tag{1}$$

Communicated by K. Mikula.

G. Chung · L. A. Vese (✉)
Department of Mathematics, University of California,
Los Angeles, CA 90095, USA
e-mail: lvese@math.ucla.edu

G. Chung
e-mail: senninha@math.ucla.edu

where $\Gamma = \cup \partial\Omega_i$, $\Omega = \cup\Omega_i \cup \Gamma$, $\mu > 0$ is a scale parameter, and $\mathcal{H}^{n-1}$ is the Hausdorff $(n-1)$-dimensional measure in $\mathbb{R}^n$. It has been shown [18] that a minimizer u of (1) has a finite number of regions Ω_i. It is easy to verify that the optimal c_i are given by $c_i = \frac{\int_{\Omega_i} f(x)dx}{|\Omega_i|}$ (when $\Omega_i \neq \emptyset$), thus the average of the data f over each Ω_i. In [18], assuming local parameterization of Γ, the Euler–Lagrange equation with respect to such local representation is also given. Thus, at points of the optimal Γ where the curve is the common boundary between two adjacent regions Ω_i and Ω_j, we must have $k = |f - c_i|^2 - |f - c_j|^2$, where k denotes the mean curvature of the common boundary.

Active contours without edges Curve evolution techniques using implicit representations [11,12,19,29] have been applied in [5,6,27] to solve particular cases of the minimal partition problem, where the number of regions Ω_i or an upper bound are assumed to be known. For instance, in [5,6] the binary case of two regions has been considered, by minimizing

$$\inf_{c_1,c_2,\phi} F(c_1, c_2, \phi) = \int_\Omega |f(x) - c_1|^2 H(\phi) dx + \int_\Omega |f(x) - c_2|^2 H(-\phi) dx + \mu \int_\Omega |\nabla H(\phi)|,$$

where c_1, c_2 are unknown constants, $\phi : \Omega \to \mathbb{R}$ is an unknown level set function, H is the one-dimensional Heaviside function, and $\int_\Omega |\nabla H(\phi)|$ denotes the total variation of the characteristic function $H(\phi)$, and represents the perimeter of the boundary of $\{x \in \Omega : \phi(x) \geq 0\}$. Minimizing the above energy as in [5,6], leads to a binary segmentation $u(x) = c_1 H(\phi(x)) + c_2 H(-\phi(x))$ of the data f, and the model acts as active contours for boundary detection. The boundary is defined implicitly by $\{x \in \Omega : \phi(x) = 0\}$. This segmentation method by curve evolution has been generalized in [27] to the case of more than two regions and to piecewise-smooth images. Using two implicit functions ϕ_1 and ϕ_2, four disjoint regions can be represented; using three functions, up to eight disjoint regions can be represented, and so on: if m level set functions are used with their corresponding zero-level lines, these can partition the domain Ω into up to 2^m disjoint regions, without vacuum or overlap. Also, triple junctions can be represented as well, with a reduced number of functions ϕ_i in [27].

Island dynamics for epitaxial growth In [2,7,14] and subsequent papers, a multilayer level set method has been applied for the modeling of island dynamics for epitaxial growth. A first layer of islands is represented by the region $\{x : \phi(x) \geq 0\}$, bounded by $\{x : \phi(x) = 0\}$; then a second layer of islands, growing on the top of the previous one is represented by $\{x : \phi(x) \geq 1\}$, bounded by $\{x : \phi(x) = 1\}$, and so on. We illustrate in Fig. 1 a one-dimensional multilayer implicit representation of islands that grow on top of each other.

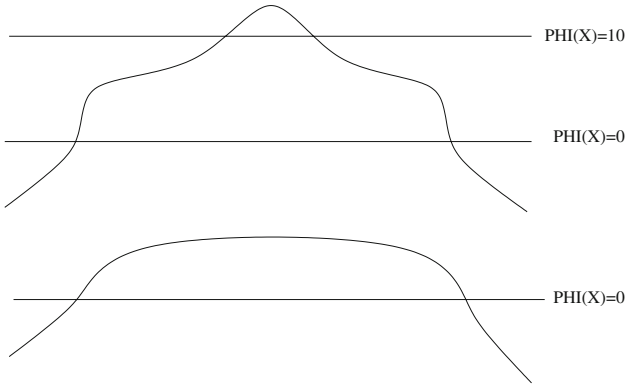

Fig. 1 *Bottom* one-dimensional plot of $\phi(x)$, and its level-line $\phi(x) = 0$ that defines a first layer of islands; *top* plot of $\phi(x)$ at a later time, with two highlighted nested level lines: $\phi(x) = 0$ and $\phi(x) = 10$, representing two layers of islands, one growing on top of the other

In summary, here we combine the techniques from [5,6,27] for image partition, with the multilayer technique for modeling epitaxial growth from [2,7,14], to obtain new and improved curve evolution models for image segmentation. Related prior work for region based segmentation using implicit curve evolution is by Cohen et al. [9,10], Paragios-Deriche [20–22], Samson et al. [24,25], Tsai et al. [26], and Tai et al. [17], among other work mentioned in [27]. A preliminary and shorter version of this work has appeared in [8]. The proposed piecewise-constant segmentation methods can be naturally extended to color image segmentation (as shown in this paper), to piecewise-polynomial or piecewise-smooth segmentation, to texture segmentation, directions and other vector-valued data segmentation.

2 Description of the proposed models

2.1 The case of one function

We consider in this subsection the case when the contours in the image f can be represented by level lines of the same implicit (Lipschitz continuous) function $\phi : \Omega \to \mathbb{R}$. Using m distinct levels $\{l_1 < l_2 < \cdots < l_m\}$, the function ϕ partitions the domain Ω into $m+1$ disjoint open regions, making up Ω, together with their boundaries:

$$R_0 = \{x \in \Omega : -\infty < \phi(x) < l_1\},$$
$$R_j = \{x \in \Omega : l_j < \phi(x) < l_{j+1}\}, \quad 1 \leq j \leq m-1$$
$$R_m = \{x \in \Omega : l_m < \phi(x) < +\infty\}.$$

We can thus extend the piecewise-constant level set segmentation models from [5,6,27], to the following model,

again as an energy minimization algorithm, in a level set form. The energy to minimize in this case, depending on $c_0, c_1, \ldots, c_m, \phi$, will be

$$\begin{aligned} F_p(c_0, c_1, \ldots, c_m, \phi) &= \int_\Omega |f(x) - c_0|^p H(l_1 - \phi(x))dx \\ &+ \sum_{j=1}^{m-1} \int_\Omega |f(x) - c_j|^p H(\phi(x) - l_j) H(l_{j+1} - \phi(x))dx \\ &+ \int_\Omega |f(x) - c_m|^p H(\phi(x) - l_m)dx \\ &+ \mu \sum_{j=1}^{m} \int_\Omega |\nabla H(\phi - l_j)|, \end{aligned}$$

where H is the one-dimensional Heaviside function, $\mu > 0$ is a weight parameter, and $p \geq 1$, thus using a more general L^p data fidelity term instead of the more standard quadratic L^2 fidelity term. Explicit minimizers c_i are obtained for $p = 2$ (appropriate for additive Gaussian noise), and for $p = 1$ [16] (appropriate for salt-and-pepper noise). The term $\int_\Omega |\nabla H(\phi - l_j)|$ represents the length of the boundary between R_j and R_{j+1}, or of the level curve $\{x \in \Omega : \phi(x) = l_j\}$ of the function ϕ.

The segmented image will be given by

$$\begin{aligned} u(x) = c_0 H(l_1 - \phi(x)) &+ \sum_{j=1}^{m-1} c_j H(\phi(x) - l_j) H(l_{j+1} - \phi(x)) \\ &+ c_m H(\phi(x) - l_m). \end{aligned}$$

To minimize the above energy, we approximate and substitute the Heaviside function H by a regularized version H_ε, as $\varepsilon \to 0$, such that $H_\varepsilon \to H$ pointwise and $H_\varepsilon \in C^1(\mathbb{R})$. We denote by $\delta_\varepsilon := H'_\varepsilon$, an approximation to the Dirac delta function δ concentrated at the origin. Examples of such approximations, that we use in practice, are [5,6]:

$$H_\varepsilon(z) = \frac{1}{2}\left(1 + \frac{2}{\pi}\arctan\left(\frac{z}{\varepsilon}\right)\right), \quad \delta_\varepsilon(z) = \frac{1}{\pi} \cdot \frac{\varepsilon}{\varepsilon^2 + z^2}.$$

To keep the notations simple, we still write in what follows H and δ (but these are assumed to be now H_ε and δ_ε, respectively). The Euler–Lagrange equations associated with the corresponding minimization

$$\inf_{c_0, c_1, \ldots, c_m, \phi} F_p(c_0, c_1, \ldots, c_m, \phi), \tag{2}$$

can be expressed as follows. In a dynamical scheme with gradient descent, starting with $\phi(0, x) = \phi_0(x)$, solve for $t > 0$, $j = 1, \ldots, m-1$,

$$\text{(if } p = 2) \begin{cases} c_0(t) = \frac{\int_\Omega f(x) H(l_1 - \phi(t,x))dx}{\int_\Omega H(l_1 - \phi(t,x))dx}, \\ c_j(t) = \frac{\int_\Omega f(x) H(\phi(t,x) - l_j) H(l_{j+1} - \phi(t,x))dx}{\int_\Omega H(\phi(t,x) - l_j) H(l_{j+1} - \phi(t,x))dx}, \\ c_m(t) = \frac{\int_\Omega f(x) H(\phi(t,x) - l_m)dx}{\int_\Omega H(\phi(t,x) - l_m)dx}, \end{cases}$$

or

$$\text{(if } p = 1) \begin{cases} c_0(t) = \text{median}_{R_0} f(x), \\ c_j(t) = \text{median}_{R_j} f(x), \\ c_m(t) = \text{median}_{R_m} f(x), \end{cases}$$

and for any $p \geq 1$,

$$\begin{aligned} \frac{\partial \phi}{\partial t} &= \delta(l_1 - \phi)|f - c_0|^p \\ &+ \sum_{j=1}^{m-1} \left[-\delta(\phi - l_j) H(l_{j+1} - \phi)|f - c_j|^p \right. \\ &\left. + \delta(l_{j+1} - \phi) H(\phi - l_j)|f - c_j|^p\right] \\ &- \delta(\phi - l_m)|f - c_m|^p \\ &+ \mu \sum_{j=1}^{m} \left[\delta(\phi - l_j) \text{div}\left(\frac{\nabla \phi}{|\nabla \phi|}\right)\right], \end{aligned}$$

$$\frac{\partial \phi}{\partial \mathbf{n}}|_{\partial\Omega} = 0,$$

where $\mathbf{n}$ is the exterior unit normal to the boundary $\partial\Omega$. Rearranging the terms, this is equivalent with

$$\begin{aligned} \frac{\partial \phi}{\partial t} &= |f - c_0|^p \delta(l_1 - \phi) \\ &+ \sum_{j=1}^{m-1} |f - c_j|^p \left[\delta(l_{j+1} - \phi) H(\phi - l_j) \right. \\ &\left. - \delta(\phi - l_j) H(l_{j+1} - \phi)\right] - |f - c_m|^p \delta(\phi - l_m) \\ &+ \mu \sum_{j=1}^{m} \left[\delta(\phi - l_j) \text{div}\left(\frac{\nabla \phi}{|\nabla \phi|}\right)\right], \end{aligned} \tag{3}$$

$$\frac{\partial \phi}{\partial \mathbf{n}}|_{\partial\Omega} = 0.$$

For a general arbitrary $p \geq 1$, the constants c_j do not have explicit expressions. If $(c_0, \ldots, c_m, \phi)$ is a minimizer of the functional, then we must have

$$\int_{R_j} |f(x) - c_j|^{p-1} \frac{f(x) - c_j}{|f(x) - c_j|} dx = 0, \quad 0 \leq j \leq m. \tag{4}$$

For $p = 2$ we thus obtain that c_j is the average (mean) of f over R_j. For $p = 1$, as in Kimmel [16], we obtain that c_j must satisfy $\int_{R_j} sign(f(x) - c_j)dx = 0$, thus we can conclude that c_j is the median of f over R_j.

We show in Fig. 2 examples of partitions of the domain Ω, using m nested level lines of a Lipschitz continuous function

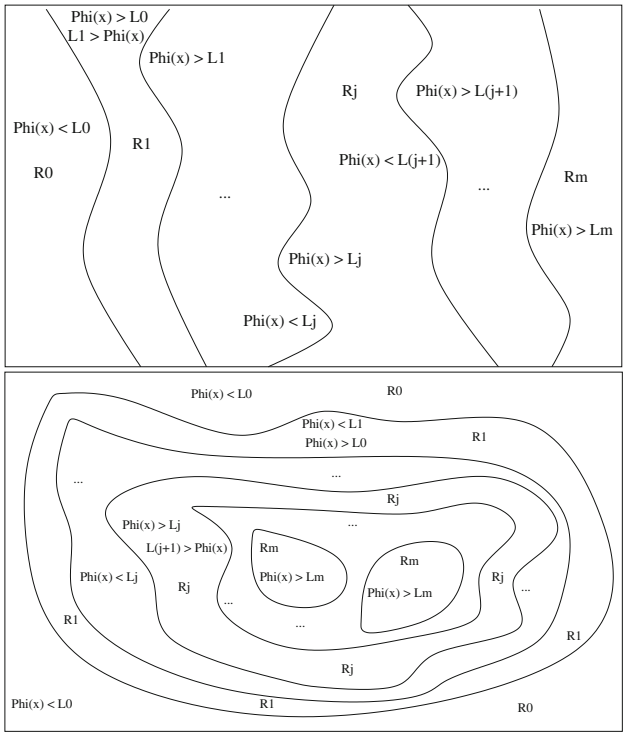

Fig. 2 Two examples of partitions of the domain Ω into $m+1$ disjoint regions, using m nested level lines $\{\phi(x) = L_i\}$ of the same function ϕ

ϕ. The particular case corresponding to $p = 2$ and $m = 2$ is discussed in details in [8].

2.1.1 Theoretical results

Energy decrease We assume in the next energy decrease result that the differentiation theorem under the integral sign can be applied and that the functions that appear are sufficiently smooth (possibly by substituting H, δ by H_ε, δ_ε, so that the differentiations and all integrals are well defined).

Theorem 1 *If $(c_0(t), c_1(t), \ldots, c_m(t), \phi(t,\cdot))$ satisfies the system of equations (3)–(4), for a given initial data ϕ_0 and $t \geq 0$, then $t \mapsto F_p(c_0(t), c_1(t), \ldots, c_m(t), \phi(t,\cdot))$ is decreasing.*

Proof We formally have

$$\begin{aligned}
&\frac{d}{dt}F_p(c_0(t), c_1(t), \ldots, c_m(t), \phi(t,\cdot)) \\
&= \int_\Omega p|f-c_0|^{p-1}\frac{f-c_0}{|f-c_0|}(-c_0'(t))H(l_1-\phi)dx \\
&\quad + \int_\Omega |f-c_0|^p\delta(l_1-\phi)(-\phi_t)dx \\
&\quad + \sum_{j=1}^{m-1}\left[\int_\Omega p|f-c_j|^{p-1}\frac{f-c_j}{|f-c_j|}(-c_j'(t))H(\phi-l_j)\right. \\
&\qquad \times H(l_{j+1}-\phi)dx + \int_\Omega |f-c_j|^p\phi_t\big(\delta(\phi-l_j)H(l_{j+1}-\phi) \\
&\qquad \left. - \delta(l_{j+1}-\phi)H(\phi-l_j)\big)\,dx\right] \\
&\quad + \int_\Omega p|f-c_m|^{p-1}\frac{f-c_m}{|f-c_m|}(-c_m'(t))H(\phi-l_m) \\
&\quad + \int_\Omega |f-c_m|^p\delta(\phi-l_m)\phi_t dx \\
&\quad + \mu\sum_{j=1}^{m}\left[\int_\Omega \delta'(\phi-l_j)\phi_t|\nabla\phi|dx\right. \\
&\quad \left. + \int_\Omega \delta(\phi-l_j)\frac{\nabla\phi\nabla\phi_t}{|\nabla\phi|}dx\right].
\end{aligned}$$

Using (4), and noticing by the boundary condition $\frac{\partial\phi(t,\cdot)}{\partial\mathbf{n}}|_{\partial\Omega} = 0$ for $t > 0$ that

$$\begin{aligned}
&\int_\Omega \delta'(\phi-l_j)\phi_t|\nabla\phi|dx + \int_\Omega \delta(\phi-l_j)\frac{\nabla\phi\nabla\phi_t}{|\nabla\phi|}dx \\
&= -\int_\Omega \delta(\phi-l_j)\phi_t\mathrm{div}\left(\frac{\nabla\phi}{|\nabla\phi|}\right)dx,
\end{aligned}$$

we obtain

$$\begin{aligned}
&\frac{d}{dt}F_p(c_0(t), c_1(t), \ldots, c_m(t), \phi(t,\cdot)) \\
&= \int_\Omega |f-c_0|^p\delta(l_1-\phi)(-\phi_t)dx \\
&\quad + \sum_{j=1}^{m-1}\int_\Omega |f-c_j|^p\phi_t\left[\delta(\phi-l_j)H(l_{j+1}-\phi)\right. \\
&\quad \left. - \delta(l_{j+1}-\phi)H(\phi-l_j)\right]dx \\
&\quad + \int_\Omega |f-c_m|^p\delta(\phi-l_m)\phi_t dx \\
&\quad - \mu\sum_{j=1}^{m}\int_\Omega \delta(\phi-l_j)\phi_t\mathrm{div}\left(\frac{\nabla\phi}{|\nabla\phi|}\right)dx \\
&= -\int_\Omega \phi_t\left\{|f-c_0|^p\delta(l_1-\phi)\right. \\
&\quad + \sum_{j=1}^{m}|f-c_j|^p\left[\delta(l_{j+1}-\phi)H(\phi-l_j)\right. \\
&\quad \left. - \delta(\phi-l_j)H(l_{j+1}-\phi)\right] - |f-c_m|^p\delta(\phi-l_m) \\
&\quad \left. + \mu\sum_{j=1}^{m}\delta(\phi-l_j)\mathrm{div}\left(\frac{\nabla\phi}{|\nabla\phi|}\right)\right\}dx.
\end{aligned}$$

Since ϕ satisfies (3), we obviously obtain that

$$\frac{d}{dt}F_p(c_0(t), c_1(t), \ldots, c_m(t), \phi(t,\cdot)) = -\int_\Omega (\phi_t)^2 dx \le 0.$$

□

Existence of minimizers We show existence of minimizers of the above functional (we limit ourselves to the case $p = 2$ for the purpose of illustration). Assume $f \in L^\infty(\Omega)$, that Ω is open, bounded, connected and with Lipschitz boundary $\partial\Omega$. Let us denote by $\chi_j = H(\phi - l_j)$, $1 \le j \le m$, where now χ_j have to be characteristic functions of sets E_j, with $E_{j+1} \subset E_j$ (this means that if $\chi_{j+1}(x) = 1$ at some point $x \in \Omega$, then $\chi_j(x) = 1$ also). This will guarantee that in the new formulation we have

$$1 - \chi_1(x) + \sum_{j=1}^{m-1} \chi_j(x)(1 - \chi_{j+1}(x)) + \chi_m(x) \equiv 1$$

for all $x \in \Omega$, i.e., a perfect partition.

Then the problem (2) for $p = 2$ can be reformulated as

$$\inf_{\chi_1, \chi_2, \ldots, \chi_m} F(\chi_1, \chi_2, \ldots, \chi_m) \tag{5}$$

where

$$\begin{aligned} F(\chi_1, \chi_2, \ldots, \chi_m) &= \int_\Omega (f - c_1(\chi_1))^2(1 - \chi_1)dx \\ &+ \sum_{j=1}^{m-1} \int_\Omega (f - c_j(\chi_j, \chi_{j+1}))^2 \chi_j(1 - \chi_{j+1})dx \\ &+ \int_\Omega (f - c_m(\chi_m))^2 \chi_m dx + \mu \sum_{j=1}^{m-1} \int_\Omega |\nabla \chi_j|, \end{aligned} \tag{6}$$

with

$$c_1(\chi_1) = \frac{\int_\Omega f(x)(1 - \chi_1)dx}{\int_\Omega (1 - \chi_1)dx},$$

$$c_j(\chi_j, \chi_{j+1}) = \frac{\int_\Omega f(x)\chi_j(1-\chi_{j+1})dx}{\int_\Omega \chi_j(1-\chi_{j+1})dx}, \quad 1 \le j \le m-1,$$

$$c_m(\chi_m) = \frac{\int_\Omega f(x)\chi_m dx}{\int_\Omega \chi_m dx}.$$

Theorem 2 *The minimization problem* (5)*, with F defined in* (6)*, has a minimizer* $(\chi_1, \ldots, \chi_m) \in BV(\Omega)^m$*, with* $\chi_j(x) \in \{0, 1\}$ *dx-a.e. for* $1 \le j \le m$*, and* $\chi_j(x) \ge \chi_{j+1}(x)$ *dx-a.e. in* Ω*.*

Proof The energy F from (6) satisfies $F \ge 0$. Also, it is easy to find characteristic functions $\chi_j = \chi_{E_j}$, $1 \le j \le m$, with $E_{j+1} \subset E_j$, E_j with finite perimeter in Ω or finite total variation in Ω, such that $F(\chi_1, \chi_2, \ldots, \chi_m) < \infty$. These two conditions on F will guarantee that the infimum is finite and therefore there is a minimizing sequence χ_j^k, such that

$$\inf_{\chi_1, \ldots, \chi_m} F(\chi_1, \ldots, \chi_m) = \lim_{k\to\infty} F(\chi_1^k, \chi_2^k, \ldots, \chi_m^k),$$

satisfying $\chi_j^k \in BV(\Omega)$, $\chi_j^k(x) \in \{0, 1\}$ dx-a.e in Ω, $\chi_j^k(x) \ge \chi_{j+1}^k(x)$ dx-a.e. in Ω.

Taking such a minimizing sequence $(\chi_1^k, \ldots, \chi_m^k)$ of F, as $k \to \infty$, among characteristic functions of sets of finite perimeter in Ω (i.e., with boundary of finite length), and since Ω is bounded, we obtain that $\|\chi_j^k\|_{BV(\Omega)} = \int_\Omega |\nabla \chi_j^k| + \|\chi_j^k\|_{L^1(\Omega)} \le M < \infty$ for any $k \ge 1$. Therefore, based on the lower semi-continuity of the total variation [13], we can extract a subsequence, still denoted by $(\chi_1^k, \ldots, \chi_m^k)$, such that each χ_i^k converges to a function $\chi_i \in BV(\Omega)$ strongly in $L^1(\Omega)$, and such that $\int_\Omega |\nabla \chi_i| \le \liminf_{k\to\infty} \int_\Omega |\nabla \chi_i^k|$. Moreover, the functions χ_j, $j = 1, \ldots, m$ have to be equal to 0 or 1 almost everywhere (due to the strong convergence in L^1, thus pointwise convergence dx.-a.e. and that $\chi_j^k \in \{0, 1\}$ dx.-a.e.), therefore these must be characteristic functions of sets of finite perimeter in Ω. We also must have in the limit, $\chi_j(x) \ge \chi_{j+1}(x)$, dx.-a.e. in Ω.

On the other hand, it is easy to verify that

$$\lim_{k\to\infty} c_1(\chi_1^k) = c_1(\chi_1),$$

$$\lim_{k\to\infty} c_j(\chi_j^k, \chi_{j+1}^k) = c_j(\chi_j, \chi_{j+1}), \quad 1 \le j \le m-1,$$

$$\lim_{k\to\infty} c_m(\chi_m^k) = c_m(\chi_1).$$

Then, we deduce that

$$F(\chi_1, \ldots, \chi_m) \le \liminf_{k\to\infty} F(\chi_1^k, \ldots, \chi_m^k),$$

therefore existence of minimizers among characteristic functions $\chi_1, \ldots, \chi_m$ of sets of finite perimeter in Ω and with $\chi_j \ge \chi_{j+1}$. □

Convergence to the length term Generalizing a result of Samson et al. [24,25], we can show that our approximating functional $L_\varepsilon(\phi) = \int_\Omega |\nabla H_\varepsilon(\phi)|dx = \int_\Omega \delta_\varepsilon(\phi)|\nabla\phi|dx$ converges to the length $|\Gamma|$ of the zero-level line $\Gamma = \{x \in \Omega : \phi(x) = 0\}$, under the assumption that $\phi : \Omega \to \mathbb{R}$ is Lipschitz. The same result holds for the case of any l-level curve of ϕ, and not only for the 0-level curve.

Theorem 3 *Let us define*

$$L_\varepsilon(\phi) = \int_\Omega |\nabla H_\varepsilon(\phi)|dx = \int_\Omega \delta_\varepsilon(\phi)|\nabla\phi|dx.$$

Then we have

$$\lim_{\varepsilon\to 0} L_\varepsilon(\phi) = \int_{\{\phi=0\}} ds = |\Gamma|,$$

where $\Gamma = \{\phi = 0\}$.

Proof Using Co-area formula [13], we have:

$$L_\varepsilon(\phi) = \int_{\mathbb{R}} \left[\int_{\phi=\rho} \delta_\varepsilon(\phi(x)) ds \right] d\rho$$
$$= \int_{\mathbb{R}} \left[\delta_\varepsilon(\rho) \int_{\phi=\rho} ds \right] d\rho.$$

By setting $h(\rho) = \int_{\phi=\rho} ds$, we obtain

$$L_\varepsilon(\phi) = \int_{\mathbb{R}} \delta_\varepsilon(\rho) h(\rho) d\rho = \int_{\mathbb{R}} \frac{1}{\pi} \frac{\varepsilon}{\varepsilon^2 + \rho^2} h(\rho) d\rho.$$

By the change of variable $\theta = \frac{\rho}{\varepsilon}$, we obtain

$$\lim_{\varepsilon \to 0} L_\varepsilon(\phi) = \lim_{\varepsilon \to 0} \int_{\mathbb{R}} \frac{1}{\pi} \frac{\varepsilon^2}{\varepsilon^2 + \varepsilon^2 \theta^2} h(\theta\varepsilon) d\theta$$
$$= \lim_{\varepsilon \to 0} \int_{\mathbb{R}} \frac{1}{\pi} \frac{1}{1+\theta^2} h(\theta\varepsilon) d\theta$$
$$= h(0) \int_{\mathbb{R}} \frac{1}{\pi} \frac{1}{1+\theta^2} d\theta$$
$$= h(0) \frac{1}{\pi} \arctan\theta |_{-\infty}^{+\infty}$$
$$= h(0) = \int_{\phi=0} ds = |\Gamma|,$$

which concludes the proof. □

In general, this convergence result is valid for any approximations H_ε, δ_ε, under the assumptions

$$\lim_{\varepsilon \to 0} H_\varepsilon(x) = H(x) \text{ in } \mathbb{R} \setminus \{0\},$$

$$\delta_\varepsilon = H_\varepsilon', H_\varepsilon \in C^1(\mathbb{R}), \int_{-\infty}^{+\infty} \delta_1(x) dx = 1.$$

2.2 The case of two functions

As in [27], we can extend the multilayer model from the previous section to the case of more than one-level set function. This may be needed for instance for images with triple junctions and with more complex structure. Let ϕ_1, ϕ_2 be two-level set functions, with distinct levels $\{l_1 < \cdots < l_m\}$ and $\{k_1 < \cdots < k_n\}$, respectively, and $m, n \geq 1$ (to simplify the notations, we introduce the conventions $l_0 = k_0 = -\infty$ and $l_{m+1} = k_{n+1} = \infty$). For $i = 0, \ldots, m$ and $j = 0, \ldots, n$, we let

$$R_{i,j} = \{x \in \Omega : \ l_i \leq \phi_1(x) \leq l_{i+1}, \ k_j \leq \phi_2(x) \leq k_{j+1}\},$$

and let $c_{i,j}$ be the unknown constant such that $f \approx c_{i,j}$ in the region $R_{i,j}$. The corresponding energy to be minimized for multilayer image segmentation, with respect to the unknowns $\mathbf{c} = (c_{i,j})_{0 \leq i \leq m,\ 0 \leq j \leq n}$, and $\Phi = (\phi_1, \phi_2)$, can be expressed as

$$F_p(\mathbf{c}, \Phi) = \sum_{i=0}^{m} \sum_{j=0}^{n} \int_\Omega |f(x) - c_{i,j}|^p H(\phi_1(x) - l_i)$$
$$\times H(l_{i+1} - \phi_1(x)) H(\phi_2(x) - k_j)$$
$$\times H(k_{j+1} - \phi_2(x)) dx$$
$$+ \mu \left[\sum_{i=1}^{m} \int_\Omega |\nabla H(\phi_1 - l_i)| dx \right.$$
$$\left. + \sum_{j=1}^{n} \int_\Omega |\nabla H(\phi_2 - k_j)| dx \right],$$

which is equivalent with

$$F_p(\mathbf{c}, \Phi) = \sum_{i=1}^{m-1} \sum_{j=1}^{n-1} \int_\Omega |f(x) - c_{i,j}|^p H(\phi_1(x) - l_i)$$
$$\times H(l_{i+1} - \phi_1(x)) H(\phi_2(x) - k_j)$$
$$\times H(k_{j+1} - \phi_2(x)) dx$$
$$+ \sum_{i=1}^{m-1} \int_\Omega |f(x) - c_{i,0}|^p H(\phi_1(x) - l_i)$$
$$\times H(l_{i+1} - \phi_1(x)) H(k_1 - \phi_2(x)) dx$$
$$+ \sum_{i=1}^{m-1} \int_\Omega |f(x) - c_{i,n}|^p H(\phi_1(x) - l_i)$$
$$\times H(l_{i+1} - \phi_1(x)) H(\phi_2(x) - k_n) dx$$
$$+ \sum_{j=1}^{n-1} \int_\Omega |f(x) - c_{0,j}|^p H(\phi_2(x) - k_j)$$
$$\times H(k_{j+1} - \phi_2(x)) H(l_1 - \phi_1(x)) dx$$
$$+ \sum_{j=1}^{n-1} \int_\Omega |f(x) - c_{m,j}|^p H(\phi_2(x) - k_j)$$
$$\times H(k_{j+1} - \phi_2(x)) H(\phi_1(x) - l_m) dx$$
$$+ \int_\Omega |f(x) - c_{0,0}|^p H(l_1 - \phi_1(x))$$
$$\times H(k_1 - \phi_2(x)) dx$$
$$+ \int_\Omega |f(x) - c_{0,n}|^p H(l_1 - \phi_1(x))$$
$$\times H(\phi_2(x) - k_n) dx$$
$$+ \int_\Omega |f(x) - c_{m,0}|^p H(\phi_1(x) - l_m)$$
$$\times H(k_1 - \phi_2(x)) dx$$
$$+ \int_\Omega |f(x) - c_{m,n}|^p H(\phi_1(x) - l_m)$$
$$\times H(\phi_2(x) - k_n) dx$$

$$+\mu\left[\sum_{i=1}^{m}\int_{\Omega}|\nabla H(\phi_1-l_i)|dx + \sum_{j=1}^{n}\int_{\Omega}|\nabla H(\phi_1-k_j)|dx\right].$$

The segmented image will be given by

$$\begin{aligned}u=&\sum_{i=1}^{m-1}\sum_{j=1}^{n-1}c_{i,j}H(\phi_1-l_i)H(l_{i+1}-\phi_1)\\&\times H(\phi_2-k_j)H(k_{j+1}-\phi_2)\\&+\sum_{i=1}^{m-1}c_{i,0}H(\phi_1-l_i)H(l_{i+1}-\phi_1)H(k_1-\phi_2)\\&+\sum_{i=1}^{m-1}c_{i,n}H(\phi_1-l_i)H(l_{i+1}-\phi_1)H(\phi_2-k_n)\\&+\sum_{j=1}^{n-1}c_{0,j}H(\phi_2-k_j)H(k_{j+1}-\phi_2)H(l_1-\phi_1)\\&+\sum_{j=1}^{n-1}c_{m,j}H(\phi_2-k_j)H(k_{j+1}-\phi_2)H(\phi_1-l_m)\\&+c_{0,0}H(l_1-\phi_1)H(k_1-\phi_2)\\&+c_{0,n}H(l_1-\phi_1)H(\phi_2-k_n)\\&+c_{m,0}H(\phi_1-l_m)H(k_1-\phi_2)\\&+c_{m,n}H(\phi_1-l_m)H(\phi_2-k_n).\end{aligned}$$

The associated Euler–Lagrange equations are, in a time-dependent gradient descent approach, with given initial guess $\phi_1(0,x)=\phi_{1,0}(x)$, $\phi_2(0,x)=\phi_{2,0}(x)$: if $p=2$, for $1\le i\le m-1$, $1\le j\le n-1$, the constants $c_{i,j}$ are explicitely given by averages (means) of f over each $R_{i,j}$,

$$\begin{aligned}&c_{i,j}(t)\\&=\frac{\int_\Omega fH(\phi_1-l_i)H(l_{i+1}-\phi_1)H(\phi_2-k_j)H(k_{j+1}-\phi_2)dx}{\int_\Omega H(\phi_1-l_i)H(l_{i+1}-\phi_1)H(\phi_2-k_j)H(k_{j+1}-\phi_2)dx},\\&c_{i,0}(t)=\frac{\int_\Omega fH(\phi_1-l_i)H(l_{i+1}-\phi_1)H(k_1-\phi_2)dx}{\int_\Omega H(\phi_1-l_i)H(l_{i+1}-\phi_1)H(k_1-\phi_2)dx},\\&c_{i,n}(t)=\frac{\int_\Omega fH(\phi_1-l_i)H(l_{i+1}-\phi_1)H(\phi_2-k_n)dx}{\int_\Omega H(\phi_1-l_i)H(l_{i+1}-\phi_1)H(\phi_2-k_n)dx},\\&c_{0,j}(t)=\frac{\int_\Omega fH(\phi_2-k_j)H(k_{j+1}-\phi_2)H(l_1-\phi_1)dx}{\int_\Omega H(\phi_2-k_j)H(k_{j+1}-\phi_2)H(l_1-\phi_1)dx},\\&c_{m,j}(t)=\frac{\int_\Omega fH(\phi_2-k_j)H(k_{j+1}-\phi_2)H(\phi_1-l_m)dx}{\int_\Omega H(\phi_2-k_j)H(k_{j+1}-\phi_2)H(\phi_1-l_m)dx},\\&c_{0,0}(t)=\frac{\int_\Omega fH(l_1-\phi_1)H(k_1-\phi_2)dx}{\int_\Omega H(l_1-\phi_1)H(k_1-\phi_2)dx},\\&c_{0,n}(t)=\frac{\int_\Omega fH(l_1-\phi_1)H(\phi_2-k_n)dx}{\int_\Omega H(l_1-\phi_1)H(\phi_2-k_n)dx},\\&c_{m,0}(t)=\frac{\int_\Omega fH(\phi_1-l_m)H(k_1-\phi_2)dx}{\int_\Omega H(\phi_1-l_m)H(k_1-\phi_2)dx},\\&c_{m,n}(t)=\frac{\int_\Omega fH(\phi_1-l_m)H(\phi_2-k_n)dx}{\int_\Omega H(\phi_1-l_m)H(\phi_2-k_n)dx}.\end{aligned}$$

For $p=1$, the constants $c_{i,j}$ are again the medians of f over the regions $R_{i,j}$, respectively:

$$c_{i,j}=\text{median}_{R_{i,j}}f(x),$$

for $0\le i\le m$, $0\le j\le n$.

For any $p\ge 1$, the unknown functions ϕ_1 and ϕ_2 are solutions of the following system of partial differential equations, obtained using gradient descent with time parameterization: given $\phi_{1,0}(x)=\phi_1(0,x)$, $\phi_{2,0}(x)=\phi_2(0,x)$, for $t>0$ solve for ϕ_1

$$\begin{aligned}\frac{\partial\phi_1}{\partial t}=&\sum_{i=1}^{m-1}\sum_{j=1}^{n-1}|f-c_{i,j}|^p\\&\times\big[-\delta(\phi_1-l_i)H(l_{i+1}-\phi_1)H(\phi_2-k_j)H(k_{j+1}-\phi_2)\\&+\delta(l_{i+1}-\phi_1)H(\phi_1-l_i)H(\phi_2-k_j)H(k_{j+1}-\phi_2)\big]\\&+\sum_{i=1}^{m-1}|f-c_{i,0}|^p\big[-\delta(\phi_1-l_i)H(l_{i+1}-\phi_1)H(k_1-\phi_2)\\&+\delta(l_{i+1}-\phi_1)H(\phi_1-l_i)H(k_1-\phi_2)\big]\\&+\sum_{i=1}^{m-1}|f-c_{i,n}|^p\big[-\delta(\phi_1-l_i)H(l_{i+1}-\phi_1)H(\phi_2-k_n)\\&+\delta(l_{i+1}-\phi_1)H(\phi_1-l_i)H(\phi_2-k_n)\big]\\&+\sum_{j=1}^{n-1}|f-c_{0,j}|^p\delta(l_1-\phi_1)H(\phi_2-k_j)H(k_{j+1}-\phi_2)\\&-\sum_{j=1}^{n-1}|f-c_{m,j}|^p\delta(\phi_1-l_m)H(\phi_2-k_j)H(k_{j+1}-\phi_2)\\&+|f-c_{0,0}|^p\delta(l_1-\phi_1)H(k_1-\phi_2)\\&+|f-c_{0,n}|^p\delta(l_1-\phi_1)H(\phi_2-k_n)\\&-|f-c_{m,0}|^p\delta(\phi_1-l_m)H(k_1-\phi_2)\\&-|f-c_{m,n}|^p\delta(\phi_1-l_m)H(\phi_2-k_n)\\&+\mu\sum_{i=1}^{m}\left[\delta(\phi_1-l_i)\text{div}\left(\frac{\nabla\phi_1}{|\nabla\phi_1|}\right)\right],\end{aligned}$$

$$\frac{\partial\phi_1}{\partial\mathbf{n}}|_{\partial\Omega}=0,$$

and for ϕ_2,

$$\begin{aligned}\frac{\partial\phi_2}{\partial t}=&\sum_{i=1}^{m-1}\sum_{j=1}^{n-1}|f-c_{i,j}|^p\\&\times\big[-\delta(\phi_2-k_j)H(k_{j+1}-\phi_2)H(\phi_1-l_i)H(l_{i+1}-\phi_1)\\&+\delta(k_{j+1}-\phi_2)H(\phi_2-k_j)H(\phi_1-l_i)H(l_{i+1}-\phi_1)\big]\end{aligned}$$

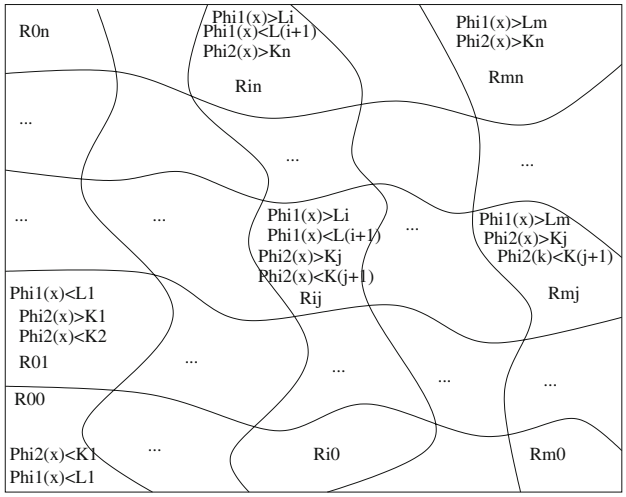

Fig. 3 Partitioning of the domain Ω into disjoint regions using level lines $\{l_1, \ldots, l_m\}$ and $\{k_1, \ldots, k_n\}$ of two functions ϕ_1 and ϕ_2, respectively

$$
\begin{aligned}
&+\sum_{j=1}^{n-1}|f-c_{0,j}|^p\left[-\delta(\phi_2-k_j)H(k_{j+1}-\phi_2)H(l_1-\phi_1)\right.\\
&\left.+\,\delta(k_{j+1}-\phi_2)H(\phi_2-k_j)H(l_1-\phi_1)\right]\\
&+\sum_{j=1}^{n-1}|f-c_{m,j}|^p\left[-\delta(\phi_2-k_j)H(k_{j+1}-\phi_2)H(\phi_1-l_m)\right.\\
&\left.+\,\delta(k_{j+1}-\phi_2)H(\phi_2-k_j)H(\phi_1-l_m)\right]\\
&+\sum_{i=1}^{m-1}|f-c_{i,0}|^p\delta(k_1-\phi_2)H(\phi_1-l_i)H(l_{i+1}-\phi_1)\\
&-\sum_{i=1}^{m-1}|f-c_{i,n}|^p\delta(\phi_2-k_n)H(\phi_1-l_i)H(l_{i+1}-\phi_1)\\
&+|f-c_{0,0}|^p\delta(k_1-\phi_2)H(l_1-\phi_1)\\
&-|f-c_{0,n}|^p\delta(\phi_2-k_n)H(l_1-\phi_1)\\
&+|f-c_{m,0}|^p\delta(k_1-\phi_2)H(\phi_1-l_m)\\
&-|f-c_{m,n}|^p\delta(\phi_2-k_n)H(\phi_1-l_m)\\
&+\mu\sum_{j=1}^{n}\left[\delta(\phi_2-k_j)\mathrm{div}\left(\frac{\nabla\phi_2}{|\nabla\phi_2|}\right)\right],
\end{aligned}
$$

$$
\frac{\partial\phi_2}{\partial\mathbf{n}}|_{\partial\Omega}=0.
$$

We show in Fig. 3 a generic example of partition of the domain Ω, using level lines corresponding to two continuous functions ϕ_1, ϕ_2. The details of the model in the case $p = 2$, $m = n = 2$ are given in [8].

The corresponding theoretical results for this case can be obtained in the same way as in the previous section. Note that, as in the multi-phase models from [27,28], when two-level set functions are used to represent the contours, as in this subsection, it is possible that two-level lines of different functions ϕ_1 and ϕ_2 may partially overlap, and therefore by the above formulation the length of the common contour will be counted more than once and will have a different weight. This is different from the Mumford and Shah energy [18]. This is not a problem in practice, as seen in the numerical approximations. Moreover, this can be simply avoided, as explained in [28].

3 Experimental results and comparisons

We show in this section experimental results applied to synthetic and real images, in the case of quadratic data fidelity terms ($p = 2$). In each figure, we show the evolution over time of the segmented image u of averages (left column), and the evolving set of curves superposed over the initial image f (right column). We also give the main parameters used in the calculations and the CPU times, together with the evolution of the energy versus iterations. We have used here a finite differences semi-implicit numerical discretization, and the details are given in the Appendix.

In Figs. 4 and 5, we illustrate how the multilayer model works on simple synthetic images without noise, using one-level set function ϕ and $m = 3$ levels. These results also illustrate the change of topology.

In Figs. 6 and 7, we illustrate how the multilayer model works on real noisy images of poor resolution, representing blood cells. Here, the model with $m = 2$ level lines of the same function ϕ has been applied, producing very satisfactory results. Note in both figures how the second-level appears during iterations, and also the automatic detection of interior contours.

We note that in all these cases, in the piecewise-constant segmentation models from [24,25,27], it would have been needed more than one function ϕ for the segmentation, therefore more computational storage would be required. In practice, we do not impose that ϕ is Lipschitz continuous. The parameter levels $l_1, l_2, \ldots$ are here kept constant and fixed for almost all our different experimental calculations. These can also be specified by the user. We have not implemented an automatic procedure of selection of these parameter levels. Sometimes, these could be estimated if a statistical prior exists about the contours or level lines of the data. We note that the algorithm is not sensitive with respect to the change of these parameter levels l_i. As in the model from [27], only an upper bound of the phases is needed. For instance we can segment an image into two regions, using the model with one-level set function and two levels (therefore with three regions in theory, but only two regions will appear in practice). Note that in all cases, the energy reaches a minimum

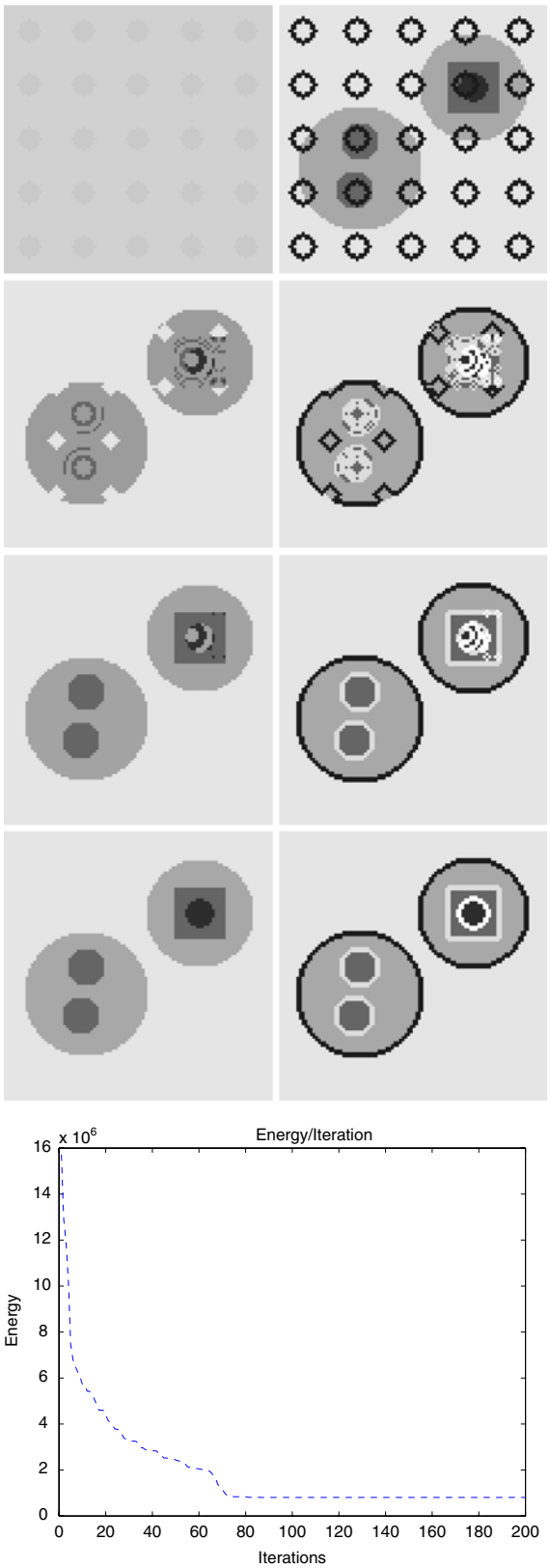

Fig. 4 Segmentation of a synthetic image of several objects with a nested structure, using one-level set function ϕ and three levels. Parameters: $l_1 = 0$, $l_2 = 25$, $l_3 = 35$, $\triangle t = 0.1$, $\mu = 0.0000511 \times 255^2$, 200 iterations, CPU time 4.015 s

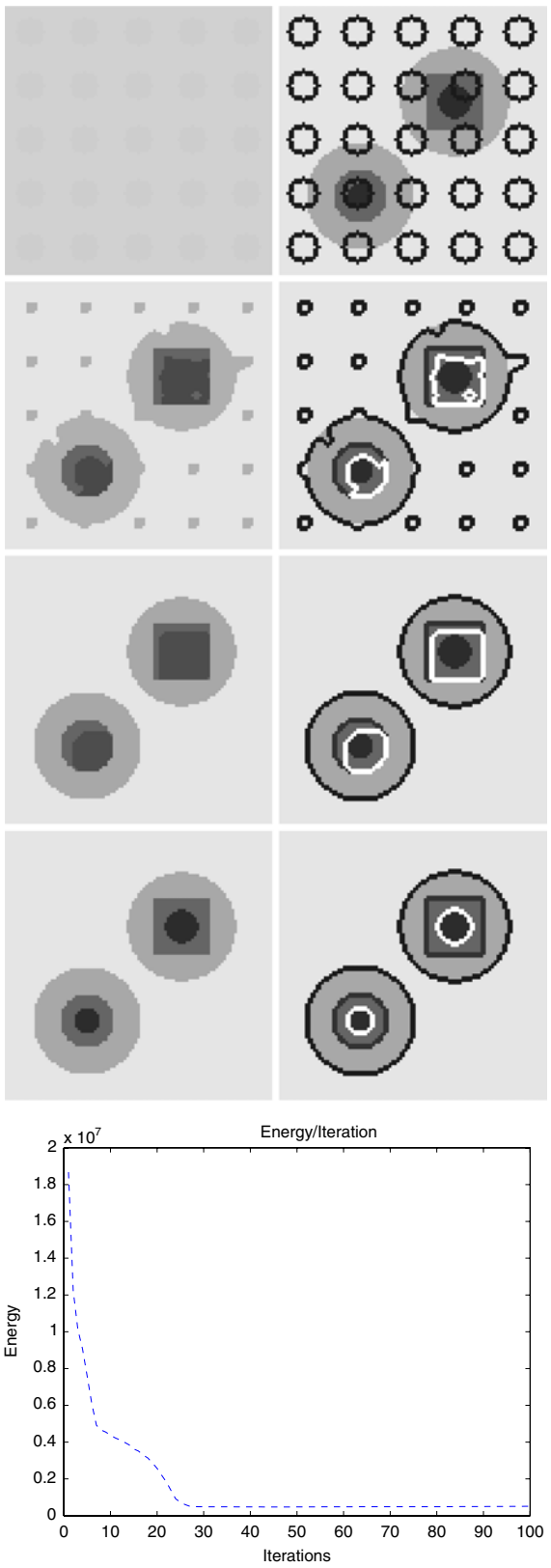

Fig. 5 Segmentation of a synthetic image of several objects with a nested structure, using one-level set function ϕ and three levels. Parameters: $l_1 = 0$, $l_2 = 25$, $l_3 = 35$, $\triangle t = 0.1$, $\mu = 0.0101 \times 255^2$, 100 iterations, CPU time 1.586 s

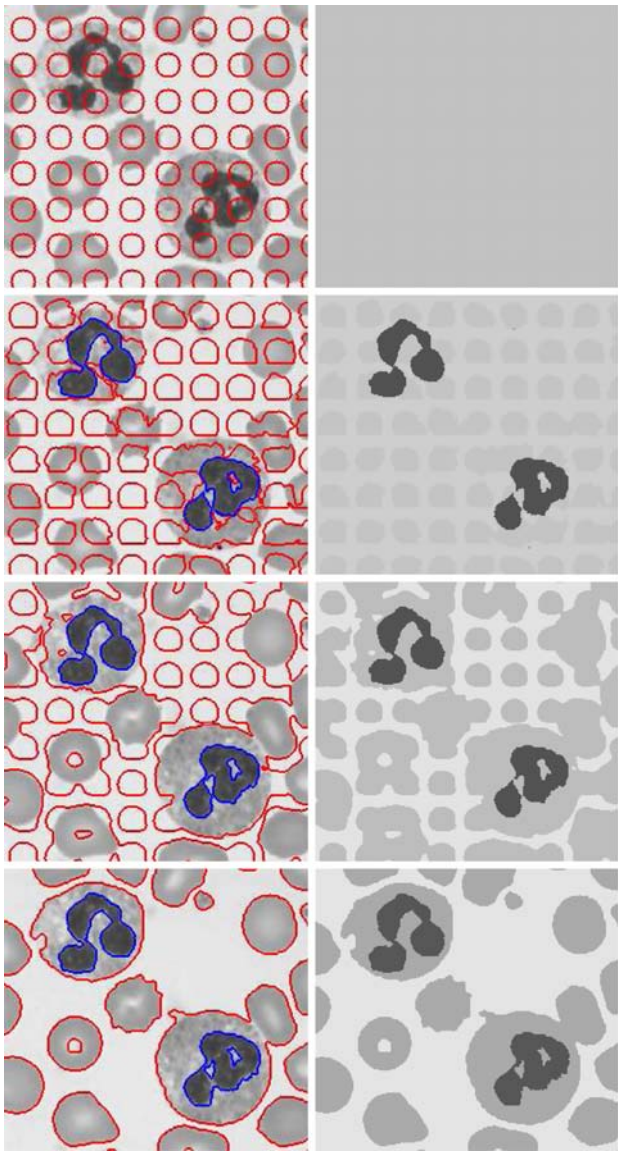

Fig. 6 Segmentation of a real blood cells image, using one-level set function ϕ and two levels. Parameters: $l_1 = 0$, $l_2 = 20$, $\triangle t = 0.5$, $\mu = 0.01$, $\nu = 0.004$ (different length term weights), 500 iterations, CPU time 68.78 s

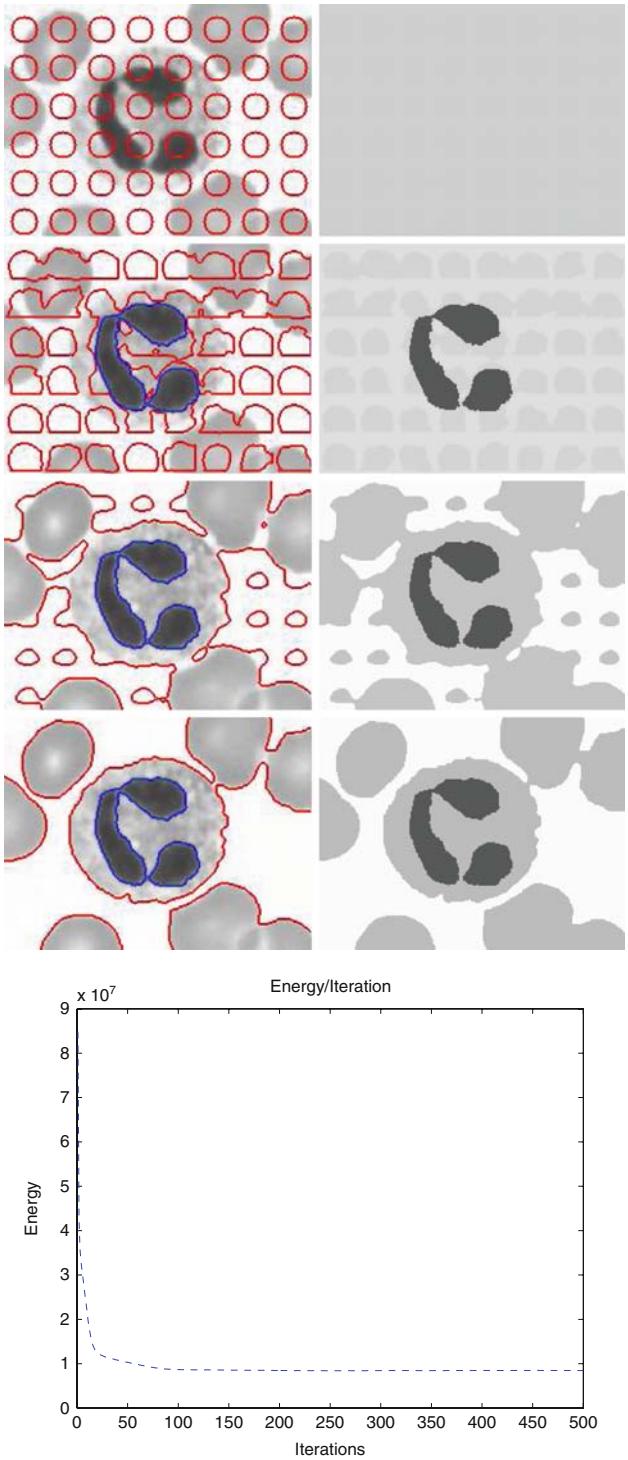

Fig. 7 Segmentation of a real blood cells image, using one-level set function ϕ and two levels. Parameters: $l_1 = 0$, $l_2 = 25$, $\triangle t = 0.5$, $\mu = 0.01$, $\nu = 0.005$ (different length term weights), 500 iterations, CPU time 68.78 s

(local or global) very fast, only after a small number of iterations. The main varying parameter in this set of results is the coefficient of the length term, which has a scaling role.

Note that in Fig. 4, during the evolution, two distinct level lines of the same function ϕ can become very close in position, almost like for a triple junction, but without overlap.

The calculations have been performed on an IBM laptop computer, in C++, with single processor of 1,600 MHz speed.

We show next numerical results on images with junctions, using our proposed new model with two functions ϕ_1, ϕ_2 and each with two levels $\{0, l\}$ (with details of the model in this case given in [8]).

We present in Fig. 8 a numerical result of segmentation and partition of a noisy synthetic image, composed of five regions of distinct intensities. All regions and corresponding intensities are correctly detected and represented. The model uses nine phases in theory, but at steady state only five appear. We also present in Fig. 9 a comparison with the multi-phase model introduced in [27] (using three level set functions). Note that the new multilayer model reaches faster the steady state, only after 40 iterations. By the previous model [27], the energy has not yet reached a steady state after 300 iterations. The CPU time comparison shows that the new model produces faster results. There is no difference in the quality of the segmentation (the RMSE's are practically the same) between the two models.

In Fig. 10 we present numerical results obtained for segmentation and partition of another real blood cells image, using two level set functions ϕ_1, ϕ_2, each with two levels $\{0, l\}$.

3.1 Color image segmentation

For color RGB images $\mathbf{f} = (f_1, f_2, f_3)$, using for example two-level set functions ϕ_1, ϕ_2, each with two levels $\{l_1 = k_1 = 0, l_2 = k_2 = l\}$, the energy is modified in the following straightforward way (see also [4]), for $p \geq 1$:

$$\begin{aligned}
&\inf_{\mathbf{c_1},\mathbf{c_2},\mathbf{c_3},\Phi} F_p(\mathbf{c_1}, \mathbf{c_2}, \mathbf{c_3}, \Phi) \\
&= \frac{1}{3}\sum_{i=1}^{3}\left\{\int_\Omega \big[|f_i(x) - c_{i,00}|^p H(-\phi_1(x))H(-\phi_2(x)) \right. \\
&\quad + |f_i(x) - c_{i,10}|^p H(\phi_1(x))H(l-\phi_1(x))H(-\phi_2(x)) \\
&\quad + |f_i(x) - c_{i,20}|^p H(\phi_1(x)-l)H(-\phi_2(x)) \\
&\quad + |f_i(x) - c_{i,01}|^p H(-\phi_1(x))H(\phi_2(x))H(l-\phi_2(x)) \\
&\quad + |f_i(x) - c_{i,11}|^p H(\phi_1(x))H(l-\phi_1(x)) \\
&\quad \times H(\phi_2(x))H(l-\phi_2(x)) \\
&\quad + |f_i(x) - c_{i,21}|^p H(\phi_1(x)-l)H(\phi_2(x))H(l-\phi_2(x)) \\
&\quad + |f_i(x) - c_{i,02}|^p H(-\phi_1(x))H(\phi_2(x)-l) \\
&\quad + |f_i(x) - c_{i,12}|^p H(\phi_1(x))H(l-\phi_1(x))H(\phi_2(x)-l) \\
&\quad \left. + |f_i(x) - c_{i,22}|^p H(\phi_1(x)-l)H(\phi_2(x)-l)\big]\,dx\right\} \\
&\quad + \mu\left[\int_\Omega |\nabla H(\phi_1)| + \int_\Omega |\nabla H(\phi_1 - l)| \right. \\
&\quad \left. + \int_\Omega |\nabla H(\phi_2)| + \int_\Omega |\nabla H(\phi_2 - l)|\right],
\end{aligned}$$

where

$$\mathbf{c_i} = (c_{i,00}, c_{i,10}, c_{i,20}, c_{i,01}, c_{i,11}, c_{i,21}, c_{i,02}, c_{i,12}, c_{i,22})$$

is the unknown vector of averages for the channel i, and $\Phi = (\phi_1, \phi_2)$ is a vector-valued unknown function of two components. The associated Euler–Lagrange equations can be written in a similar way, embedding the minimization in a dynamical scheme, and starting with $\phi_1(0, x) = \phi_{1,0}(x)$, $\phi_2(0, x) = \phi_{2,0}(x)$. We have that for $p = 2$, the unknown constants $c_{i,kl}$ are given by the averages of the data f_i on their corresponding regions $R_{i,kl}$, $1 \leq i \leq 3$, $0 \leq k, l \leq 2$, as follows:

$$\begin{aligned}
c_{i,00}(t) &= \frac{\int_\Omega f_i H(-\phi_1)H(-\phi_2)dx}{\int_\Omega H(-\phi_1)H(-\phi_2)dx}, \\
c_{i,10}(t) &= \frac{\int_\Omega f_i H(\phi_1)H(l-\phi_1)H(-\phi_2)dx}{\int_\Omega H(\phi_1)H(l-\phi_1)H(-\phi_2)dx}, \\
c_{i,20}(t) &= \frac{\int_\Omega f_i H(\phi_1-l)H(-\phi_2)dx}{\int_\Omega H(\phi_1-l)H(-\phi_2)dx}, \\
c_{i,01}(t) &= \frac{\int_\Omega f_i H(-\phi_1)H(\phi_2)H(l-\phi_2)dx}{\int_\Omega H(-\phi_1)H(\phi_2)H(l-\phi_2)dx}, \\
c_{i,11}(t) &= \frac{\int_\Omega f_i H(\phi_1)H(\phi_2)H(l-\phi_1)H(l-\phi_2)dx}{\int_\Omega H(\phi_1)H(\phi_2)H(l-\phi_1)H(l-\phi_2)dx}, \\
c_{i,21}(t) &= \frac{\int_\Omega f_i H(\phi_1-l)H(\phi_2)H(l-\phi_2)dx}{\int_\Omega H(\phi_1-l)H(\phi_2)H(l-\phi_2)dx}, \\
c_{i,02}(t) &= \frac{\int_\Omega f_i H(-\phi_1)H(\phi_2-l)dx}{\int_\Omega H(-\phi_1)H(\phi_2-l)dx}, \\
c_{i,12}(t) &= \frac{\int_\Omega f_i H(\phi_1)H(l-\phi_1)H(\phi_2-l)dx}{\int_\Omega H(\phi_1)H(l-\phi_1)H(\phi_2-l)dx}, \\
c_{i,22}(t) &= \frac{\int_\Omega f_i H(\phi_1-l)H(\phi_2-l)dx}{\int_\Omega H(\phi_1-l)H(\phi_2-l)dx},
\end{aligned}$$

while for $p = 1$ these are the medians of f_i over the same corresponding regions $R_{i,kl}$.

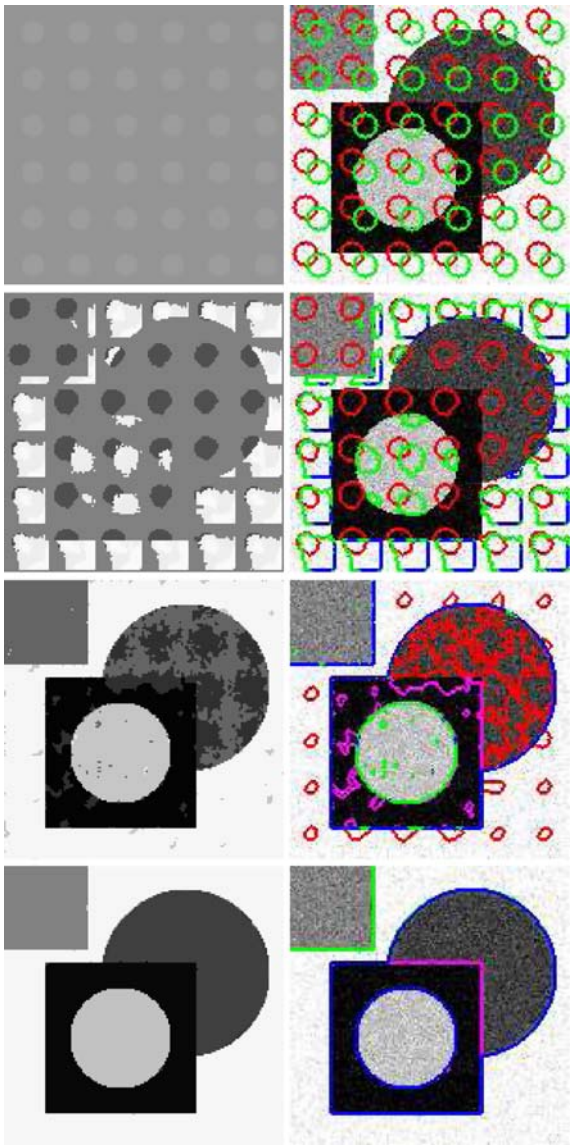

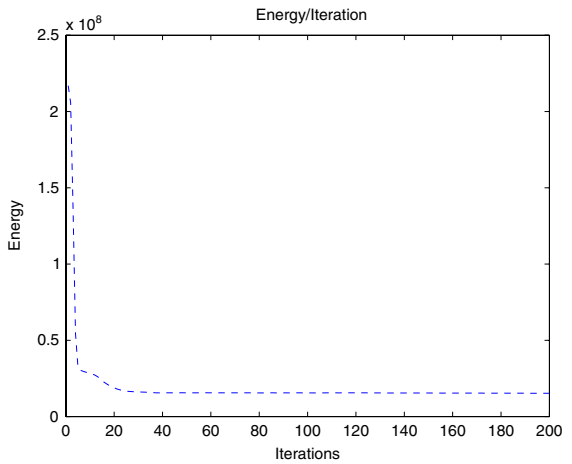

Fig. 8 Segmentation of a noisy synthetic image with triple junctions, using two functions ϕ_1, ϕ_2 and two levels. Parameters: $l_1 = 0, l_2 = 25$, $\triangle t = 0.4$, $\mu = 0.023 \times 255^2$, 200 iterations, CPU time 13.985 s, RMSE = 52.3226

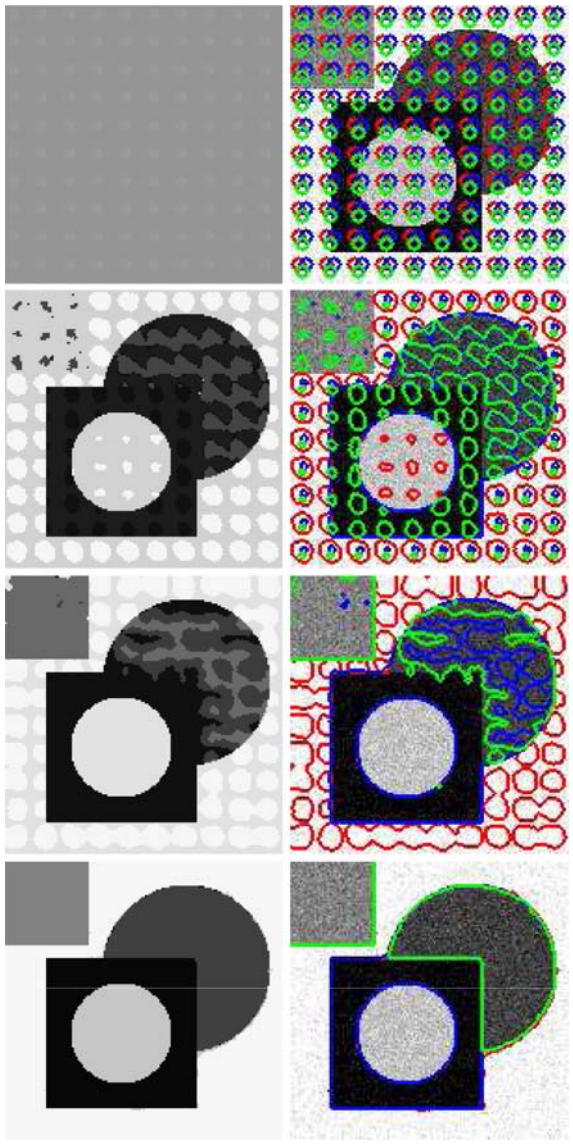

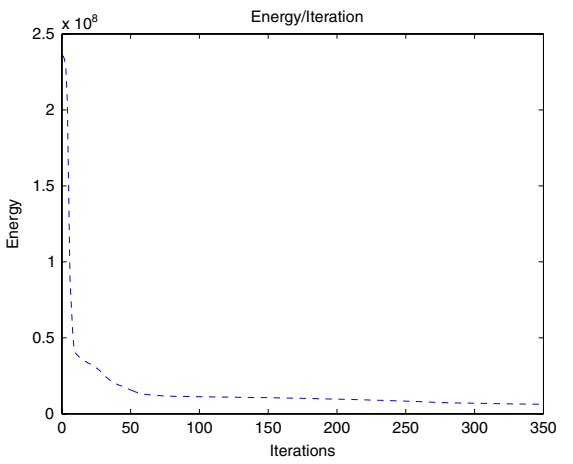

Fig. 9 Segmentation obtained using the model from [27], using three-level set functions (eight phases), each zero-level-line of ϕ_i representing a curve. Parameters: $l = 0$, $\triangle t = 0.4$, $\mu = 0.06 \times 255^2$, 350 iterations, CPU time 30.967 s, RMSE = 52.70172

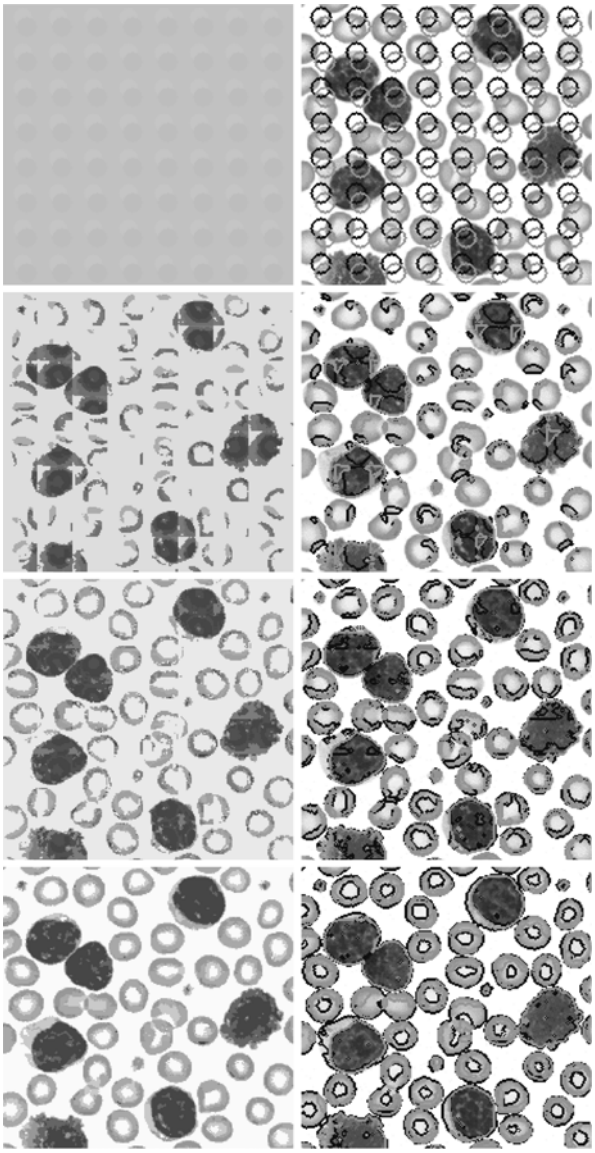

Fig. 10 Segmentation of a real blood cells image with junctions, using two functions ϕ_1, ϕ_2 and two levels. Parameters: $l_1 = 0$, $l_2 = 25$, $\triangle t = 0.4$, $\mu = 0.05 \times 255^2$, 100 iterations, CPU time 10.814 s

For any $p \geq 1$, the unknown functions ϕ_1 and ϕ_2 are solutions of the following equations:

$$\phi_1(0,x) = \phi_{1,0}(x), \quad \phi_2(0,x) = \phi_{2,0}(x),$$

$$\begin{aligned}
\frac{\partial \phi_1}{\partial t} = \delta_\varepsilon(\phi_1) \Bigg\{ & \frac{1}{3}\sum_{i=1}^{3} \Big[|f - c_{i,00}|^p H(-\phi_2) \\
& - |f - c_{i,10}|^p H(l - \phi_1) H(-\phi_2) \\
& + |f - c_{i,01}|^p H(\phi_2) H(l - \phi_2) \\
& - |f - c_{i,11}|^p H(l - \phi_1) H(\phi_2) H(l - \phi_2) \\
& + |f - c_{i,02}|^p H(\phi_2 - l) \\
& - |f - c_{i,12}|^p H(l - \phi_1) H(\phi_2 - l) \Big] + \mu \operatorname{div}\left(\frac{\nabla \phi_1}{|\nabla \phi_1|} \right) \Bigg\} \\
& + \delta_\varepsilon(\phi_1 - l) \Bigg\{ \frac{1}{3}\sum_{i=1}^{3} \Big[|f - c_{i,10}|^p H(\phi_1) H(-\phi_2) \\
& - |f - c_{i,20}|^p H(-\phi_2) \\
& + |f - c_{i,11}|^p H(\phi_1) H(\phi_2) H(l - \phi_2) \\
& - |f - c_{i,21}|^p H(\phi_2) H(l - \phi_2) \\
& + |f - c_{i,12}|^p H(\phi_1) H(\phi_2 - l) \\
& - |f - c_{i,22}|^p H(\phi_2 - l) \Big] + \mu \operatorname{div}\left(\frac{\nabla \phi_1}{|\nabla \phi_1|} \right) \Bigg\},
\end{aligned}$$

$$\begin{aligned}
\frac{\partial \phi_2}{\partial t} = \delta_\varepsilon(\phi_2) \Bigg\{ & \frac{1}{3}\sum_{i=1}^{3} \Big[|f - c_{i,00}|^p H(-\phi_1) \\
& - |f - c_{i,01}|^p H(-\phi_1) H(l - \phi_2) \\
& + |f - c_{i,10}|^p H(\phi_1) H(l - \phi_1) \\
& - |f - c_{i,11}|^p H(\phi_1) H(l - \phi_1) H(l - \phi_2) \\
& + |f - c_{i,20}|^p H(\phi_1 - l) \\
& - |f - c_{i,21}|^p H(\phi_1 - l) H(l - \phi_2) \Big] + \mu \operatorname{div}\left(\frac{\nabla \phi_2}{|\nabla \phi_2|} \right) \Bigg\} \\
& + \delta_\varepsilon(\phi_2 - l) \Bigg\{ \frac{1}{3}\sum_{i=1}^{3} \Big[|f - c_{i,01}|^p H(-\phi_1) H(\phi_2) \\
& - |f - c_{i,02}|^p H(-\phi_1) \\
& + |f - c_{i,11}|^p H(\phi_1) H(l - \phi_1) H(\phi_2) \\
& - |f - c_{i,12}|^p H(\phi_1) H(l - \phi_1) \\
& + |f - c_{i,21}|^p H(\phi_1 - l) H(\phi_2) \\
& - |f - c_{i,22}|^p H(\phi_1 - l) \Big] + \mu \operatorname{div}\left(\frac{\nabla \phi_2}{|\nabla \phi_2|} \right) \Bigg\}.
\end{aligned}$$

In Fig. 11 we show a numerical result, taken from [8], of a noisy synthetic color image consisting of 9 regions of distinct intensities. This can be seen as an extension of the work [4].

4 The choice of curve regularization

In the previous sections, the regularization on the level lines $\{\phi(x) = l_i\}$ was imposed by penalizing the length of contours, in the spirit of the Mumford and Shah functional [18] (in fact, this corresponds to the counting measure in one dimension, the length measure in two dimensions, and the surface area measure in three dimensions). Thus, for the case of one function ϕ with m levels, the geometric regularization was of the form:

- Length regularization:

$$\mathcal{R}(\phi) = \mu \sum_{i=1}^{m} \int_{\Omega} |\nabla H(\phi - l_i)| dx,$$

that gives the following term in the Euler–Lagrange equation:

$$\frac{\partial \phi}{\partial t} = (\text{fidelity terms}) + \mu \sum_{i=1}^{m} \delta(\phi - l_i) \text{div}\left(\frac{\nabla \phi}{|\nabla \phi|}\right).$$

We discuss and propose here other regularizations, that act on all level lines $\{\phi(x) = l_i\}$, as follows:

- Total variation regularization as in image restoration [23]

$$\mathcal{R}(\phi) = \mu \int_{\Omega} |\nabla \phi| dx,$$

that gives the following term in the Euler–Lagrange equation:

$$\frac{\partial \phi}{\partial t} = (\text{fidelity terms}) + \mu \ \text{div}\left(\frac{\nabla \phi}{|\nabla \phi|}\right),$$

or smoothing only in the tangent direction of each level line.

- Mean curvature regularization [19], directly in the PDE form,

$$\frac{\partial \phi}{\partial t} = (\text{fidelity terms}) + \mu |\nabla \phi| \text{div}\left(\frac{\nabla \phi}{|\nabla \phi|}\right).$$

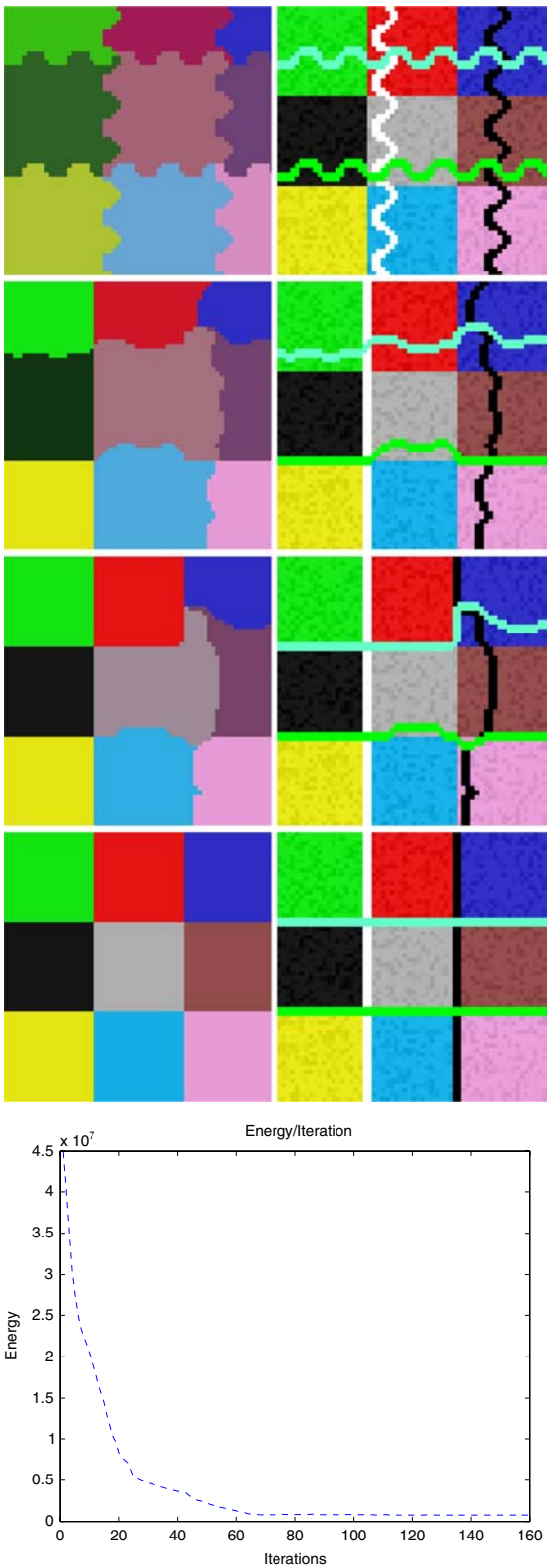

Fig. 11 Segmentation of noisy synthetic color image with junctions, using two functions ϕ_1, ϕ_2 and two levels. Parameters: $l_1 = 0, l_2 = 25$, $\triangle t = 0.01$, $\mu = 0.335 \times 255^2$, 160 iterations, CPU time 10.975 s. Note that the image contains nine different regions, all correctly detected and segmented in an efficient approach

- H^1 regularization

$$\mathcal{R}(\phi) = \mu \int_{\Omega} |\nabla \phi|^2 dx,$$

that gives the following term in the Euler–Lagrange equation:

$$\frac{\partial \phi}{\partial t} = (\text{fidelity terms}) + 2\mu \triangle \phi,$$

in other words pure isotropic smoothing at every point x.

- Sup-norm of the gradient regularization or $W^{1,\infty}$ regularization (also called AMLE, "absolutely minimizing Lipschitz extensions"):

$$\mathcal{R}(\phi) = \mu \| |\nabla \phi| \|_{L^\infty(\Omega)},$$

that gives the following term in the Euler–Lagrange equation:

$$\frac{\partial \phi}{\partial t} = (\text{fidelity terms}) + \mu \triangle_\infty \phi,$$

where $\triangle_\infty \phi = D^2\phi(\frac{\nabla\phi}{|\nabla\phi|}, \frac{\nabla\phi}{|\nabla\phi|})$ is the normalized infinity Laplacian. We refer to [1,3,15] for the derivation of this differential equation and applications (note that the functional is no longer of integral form, so the Euler–Lagrange equation cannot be directly computed). This smoothing of ϕ, only in the normal direction of level lines of ϕ, is the strongest one among those mentioned above.

We illustrate in Figs. 12, 13, 14, 15, and 16 the effect of using these regularizations for the function ϕ, in the model with one-level set function and $m = 3$ levels, all applied to the segmentation of a synthetic noisy image with concentric geometric objects (we do not show the evolution over iterations, we only show the steady states). In all cases, we show the final levels l_1, l_2, l_3 of ϕ over the original image f, the piecewise-constant segmented image u of averages, a contour plot of ϕ (every ten levels), and the surface graph of the function ϕ. We see that in the case of length regularization or TV regularization, the level set function, as expected, is not continuous and its level lines tend to overlap; while with the smoother regularizations H^1 or $W^{1,\infty}$, the function ϕ as expected remains continuous, and the contour plot shows, especially in the case of the $W^{1,\infty}$ regularization, that the level lines are more equally spread, as for a signed-distance function. However, there is no need of re-initialization to the distance function. Higher-order regularizations could have been used, coming from a bending energy term.

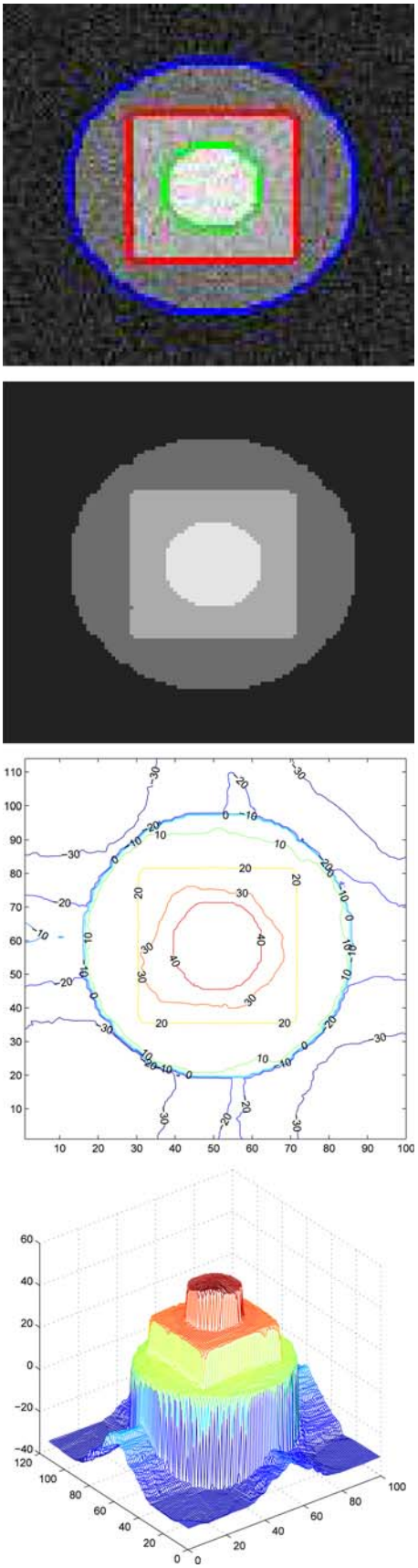

Fig. 12 Results using length regularization

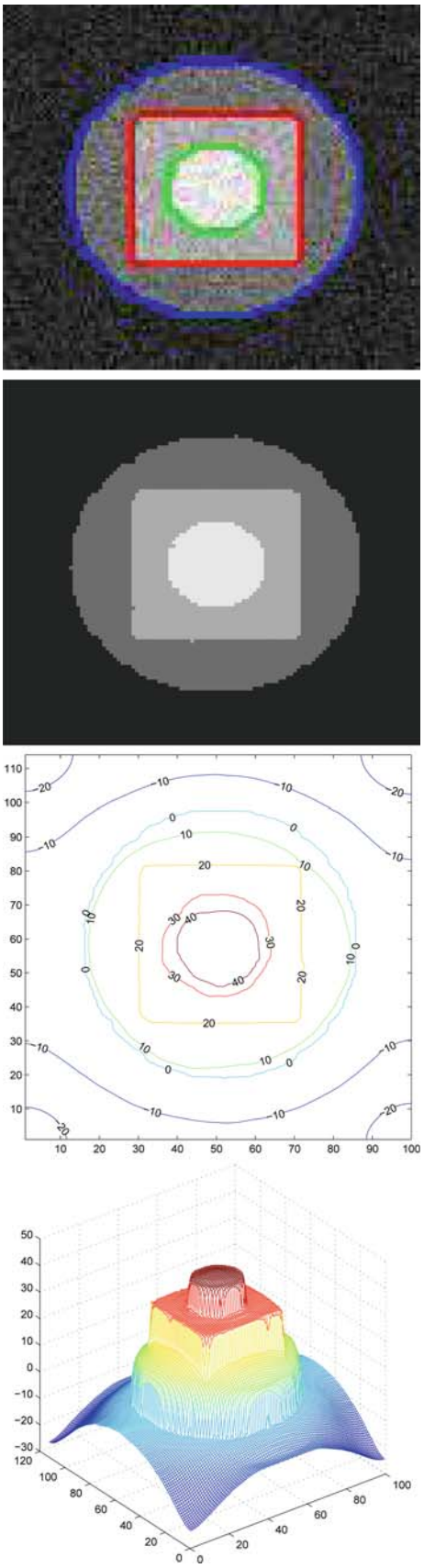

Fig. 13 Results using TV regularization

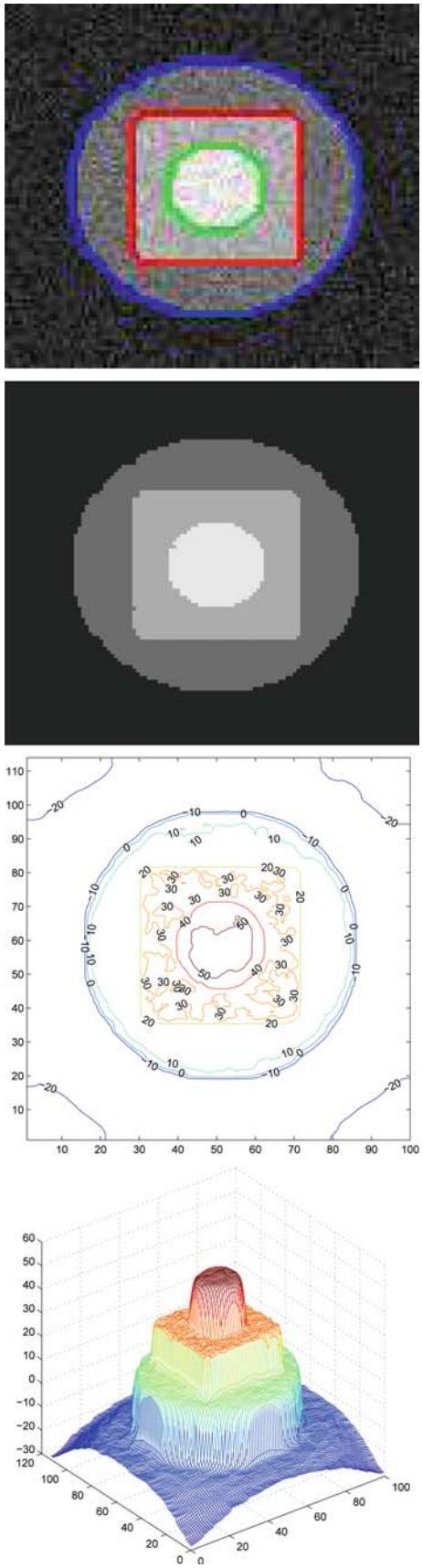

Fig. 14 Results using mean curvature motion regularization

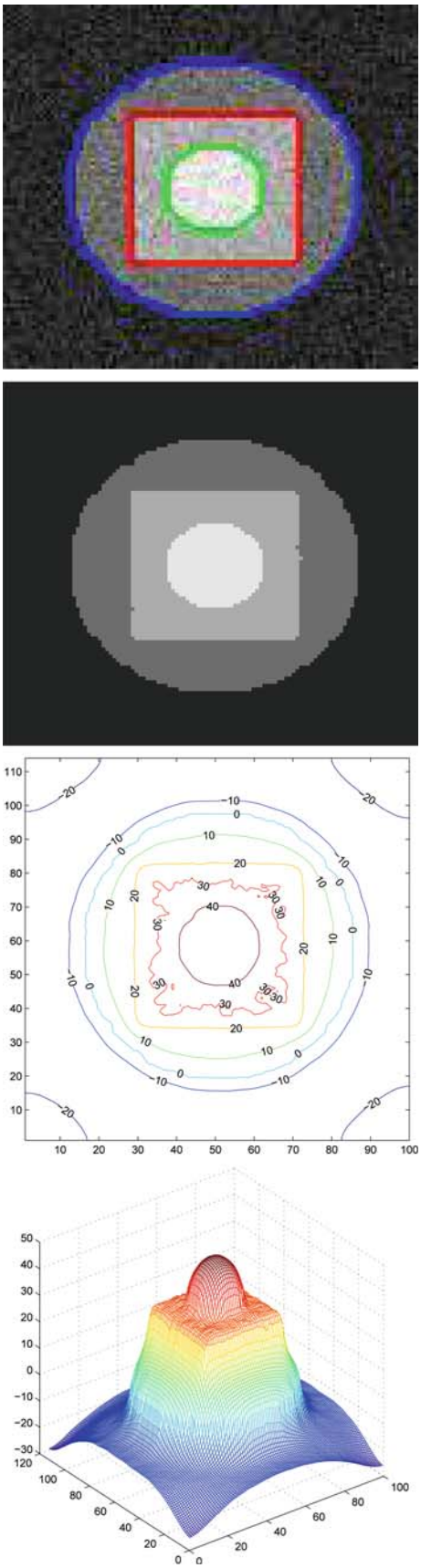

Fig. 15 Results using H^1 regularization

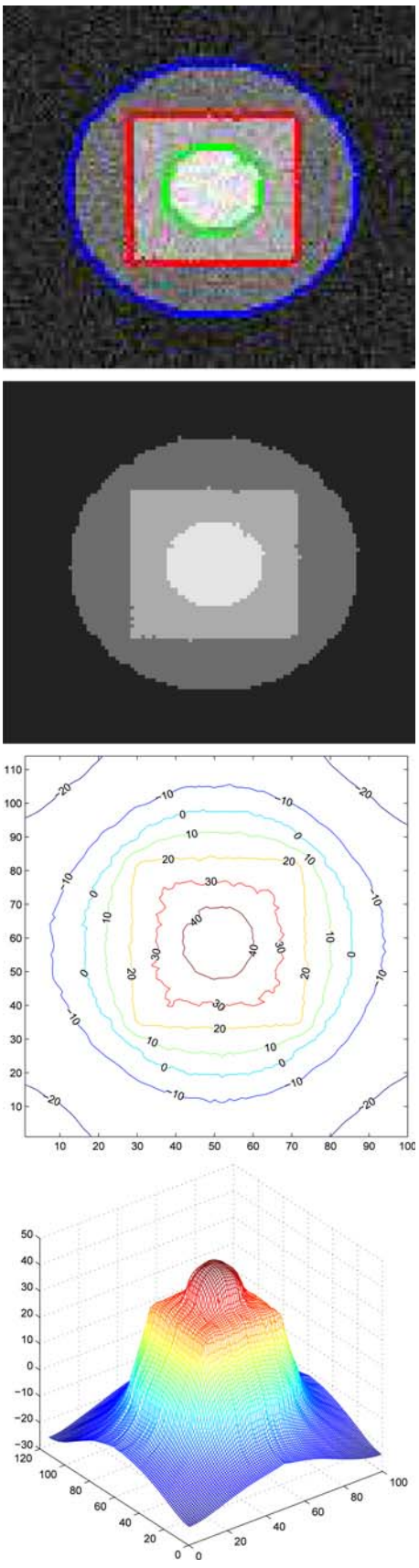

Fig. 16 Results using sup-norm of the gradient regularization

Acknowledgements The authors would like to thank the guest editor Karol Mikula for the invitation to contribute to this special issue. Also, the authors would like to thank the unknown referee for his (her) useful comments, suggestions and corrections. Finally, this work has been supported in part by an Alfred P. Sloan fellowship, by the National Institute of Health through the NIH Roadmap for Medical Research: Grant U54 RR021813 entitled Center for Computational Biology CCB, by the National Science Foundation Grants NSF ITR 0113439 and NSF DMS 0312222, and by the Institute for Pure and Applied Mathematics.

Appendix

Description of the numerical algorithm We give here the details of our numerical algorithm in two dimensions, in the case of one function ϕ with two levels $\{l_1 = 0, l_2 = l > 0\}$ and $p = 2$. Let h be the space step, $\triangle t$ be the time step, and $\varepsilon = h$. Let (x_i, y_j) be the discrete points, for $1 \le i, j \le M$, and $f_{i,j} \approx f(x_i, y_j)$, $\phi^n_{i,j} \approx \phi(n\triangle t, x_i, y_j)$, with $n \ge 0$. Recall the usual finite differences formulas

$$\begin{aligned}
\triangle^x_+ \phi_{i,j} &= \phi_{i+1,j} - \phi_{i,j},\\
\triangle^x_- \phi_{i,j} &= \phi_{i,j} - \phi_{i-1,j},\\
\triangle^y_+ \phi_{i,j} &= \phi_{i,j+1} - \phi_{i,j},\\
\triangle^y_- \phi_{i,j} &= \phi_{i,j} - \phi_{i,j-1}.
\end{aligned}$$

Set $n = 0$, and start with $\phi^0_{i,j}$ given (defining the initial set of curves). Then, for each $n > 0$ until steady state:

1) compute averages $c^n_1 \approx c_1(n\triangle t)$, $c^n_2 \approx c_2(n\triangle t)$, and $c^n_3 \approx c_3(n\triangle t)$.
2) compute $\phi^{n+1}_{i,j}$, derived from the finite differences scheme:

$$\begin{aligned}
\frac{\phi^{n+1}_{i,j} - \phi^n_{i,j}}{\triangle t} &= \delta_\varepsilon(\phi^n_{i,j}) \left[\frac{\mu}{h^2} \left(\triangle^x_- \left(\frac{\phi^n_{i+1,j} - \phi^{n+1}_{i,j}}{|\nabla \phi^n_{i,j}|} \right) \right.\right.\\
&\quad \left.\left. + \triangle^y_- \left(\frac{\phi^n_{i,j+1} - \phi^{n+1}_{i,j}}{|\nabla \phi^n_{i,j}|} \right) \right) \right.\\
&\quad \left. + |f_{i,j} - c^n_1|^2 - |f_{i,j} - c^n_2|^2 H_\varepsilon(l - \phi^n_{i,j}) \right]\\
&\quad + \delta_\varepsilon(\phi^n_{i,j} - l) \left[\frac{\mu}{h^2} \left(\triangle^x_- \left(\frac{\phi^n_{i+1,j} - \phi^{n+1}_{i,j}}{|\nabla \phi^n_{i,j}|} \right) \right.\right.\\
&\quad \left.\left. + \triangle^y_- \left(\frac{\phi^n_{i,j+1} - \phi^{n+1}_{i,j}}{|\nabla \phi^n_{i,j}|} \right) \right) \right.\\
&\quad \left. - |f_{i,j} - c^n_3|^2 + |f_{i,j} - c^n_2|^2 H_\varepsilon(\phi^n_{i,j}) \right],
\end{aligned}$$

where $|\nabla \phi^n_{i,j}| = \sqrt{\left(\frac{\phi^n_{i+1,j} - \phi^n_{i,j}}{h} \right)^2 + \left(\frac{\phi^n_{i,j+1} - \phi^n_{i,j}}{h} \right)^2}$. Let

$$\begin{aligned}
C_1 &= \frac{1}{\sqrt{\left(\frac{\phi^n_{i+1,j} - \phi^n_{i,j}}{h} \right)^2 + \left(\frac{\phi^n_{i,j+1} - \phi^n_{i,j}}{h} \right)^2}},\\
C_2 &= \frac{1}{\sqrt{\left(\frac{\phi^n_{i,j} - \phi^n_{i-1,j}}{h} \right)^2 + \left(\frac{\phi^n_{i-1,j+1} - \phi^n_{i-1,j}}{h} \right)^2}},\\
C_3 &= \frac{1}{\sqrt{\left(\frac{\phi^n_{i+1,j} - \phi^n_{i,j}}{h} \right)^2 + \left(\frac{\phi^n_{i,j+1} - \phi^n_{i,j}}{h} \right)^2}},\\
C_4 &= \frac{1}{\sqrt{\left(\frac{\phi^n_{i+1,j-1} - \phi^n_{i,j-1}}{h} \right)^2 + \left(\frac{\phi^n_{i,j} - \phi^n_{i,j-1}}{h} \right)^2}}.
\end{aligned}$$

Let $m_1 = \frac{\triangle t}{h^2}(\delta_\varepsilon(\phi^n_{i,j}) + \delta_\varepsilon(\phi^n_{i,j} - l))\mu$, $C = 1 + m_1(C_1 + C_2 + C_3 + C_4)$. The main update equation for ϕ becomes

$$\begin{aligned}
\phi^{n+1}_{i,j} = \frac{1}{C} \Big[& \phi^n_{i,j} + m_1(C_1 \phi^n_{i+1,j} + C_2 \phi^n_{i-1,j}\\
& + C_3 \phi^n_{i,j+1} + C_4 \phi^n_{i,j-1})\\
& + \triangle t \delta_\varepsilon(\phi^n_{i,j})(-(f_{i,j} - c^n_2)^2 (1 - H_\varepsilon(\phi^n_{i,j} - l))\\
& + (f_{i,j} - c^n_3)^2) + \triangle t \delta_\varepsilon(\phi^n_{i,j} - l)(-(f_{i,j} - c^n_1)^2\\
& + (f_{i,j} - c^n_2)^2 H_\varepsilon(\phi^n_{i,j})) \Big],
\end{aligned}$$

and repeat, until steady state is reached.

References

1. Aronsson, G.: Extension of functions satisfying Lipschitz conditions. Ark. Mat. **6**(6), 551–561 (1967)
2. Caflisch, R.E., Gyure, M.F., Merriman, B., Osher, S., Ratsch, C., Vvedensky, D.D., Zinck, J.J.: Island dynamics and the level set method for epitaxial growth. Appl. Math. Lett. **12**(4), 13 (1999)
3. Caselles, V., Morel, J.-M., Sbert, C.: An axiomatic approach to image interpolation. IEEE Trans. Image Process. **7**(3), 376–386 (1998)
4. Chan, T.F., Sandberg, B.Y., Vese, L.A.: Active contours without edges for vector-valued images. J. Vis. Commun. Image Represent. **11**(2), 130–141 (2000)
5. Chan, T.F., Vese, L.: An active contour model without edges. In: Scale-Space Theories in Computer Vision, Lecture Notes in Computer Science, Vol. 1682, pp. 141–151 (1999)
6. Chan, T.F., Vese, L.A.: Active contours without edges. IEEE Trans. Image Process. **10**(2), 266–277 (2001)
7. Chen, S., Kang, M., Merriman, B., Caflisch, R.E., Ratsch, C., Fedkiw, R., Gyure, M.F., Osher, S.: Level set method for thin film epitaxial growth. J. Comput. Phys. **167**, 475 (2001)
8. Chung, G., Vese, L.A.: Energy minimization based segmentation and denoising using a multilayer level set approach. In: Rangarajan, A., Vemuri, B., Yuille, A.L. (eds.) Energy Minimization Methods in

Computer Vision and Pattern Recognition, 5th International Workshop, EMMCVPR 2005, St Augustine, FL, USA, 9–11 November 2005. LNCS, Vol. 3757/2005, pp. 439–455 (2005)
9. Cohen, L.D.: Avoiding local minima for deformable curves in image analysis. In: Le Méhauté, A., Rabut, C., Schumaker L.L. (eds.) Curves and Surfaces with Applications in CAGD, pp. 77–84 (1997)
10. Cohen, L., Bardinet, E., Ayache, N.: Surface reconstruction using active contour models. In: Proceedings of SPIE 93 Conference on Geometric Methods in Computer Vision, San Diego (1993)
11. Dervieux, A., Thomasset, F.: A finite element method for the simulation of Rayleigh–Taylor instability. Lect. Notes Math. **771**, 145–159 (1979)
12. Dervieux, A., Thomasset, F.: Multifluid incompressible flows by a finite element method. Lect. Notes Phys. **141**, 158–163 (1980)
13. Evans L.C., Gariepy, R.: Measure Theory and Fine Properties of Functions. CRC Press, London (1992)
14. Gyure, M.F., Ratsch, C., Merriman, B., Caflisch, R.E., Osher, S., Zinck, J.J., Vvedensky, D.D.: Level set methods for the simulation of epitaxial phenomena. Phys. Rev. E **58**, R6927 (1998)
15. Jensen, R.: Uniqueness of Lipschitz extensions—minimizing the sup norm of the gradient. Arch. Ration. Mech. Anal. **123**(1), 51–74 (1993)
16. Kimmel, R.: Fast Edge Integration. In: Osher S., Paragios N. (eds) Geometric Level Set Methods in Imaging, Vision and Graphics, pp.59–77. Springer, Heidelberg (2003)
17. Lie, J., Lysaker, M., Tai, X.-C.: A Binary Level Set Model and Some Applications to Mumford-Shah Image Segmentation. IEEE Trans. Image Process. **15**(5), 1171–1181 (2006)
18. Mumford, D., Shah, J.: Optimal approximation by piecewise smooth functions and associated variational problems. Comm. Pure Appl. Math. **42**, 577–685 (1989)
19. Osher, S., Sethian, J.: Fronts propagating with curvature-dependent speed—algorithms based on Hamilton–Jacobi formulations. JCP **79**(1), 12–49 (1988)
20. Paragios, N., Deriche, R.: Unifying boundary and region-based information for geodesic active tracking. Proc. Comput. Vision Pattern Recognit. **2**,23–25 (1999)
21. Paragios, N., Deriche, R.: Geodesic active regions: a new framework to deal with frame partition problems in computer vision. J. Vis. Commun. Image Represent. **13**(1–2), 249–268 (2002)
22. Paragios, N., Deriche, R.: Geodesic active regions and level set methods for supervised texture segmentation. IJCV **46**(3), 223–247 (2002)
23. Rudin, L.I., Osher, S., Fatemi, E.: Nonlinear Total variation based noise removal algorithms. Phys. D Nonlinear Phenomena **60**(1–4), 259–268 (1992)
24. Samson, C., Blanc-Féraud, L., Aubert, G., Zérubia, J.: A Level Set Model for Image Classification. LNCS, vol. 1682, pp. 306–317
25. Samson, C., Blanc-Féraud, L., Aubert, G., Zérubia, J.: A level set model for image classification. IJCV **40**(3), 187–197 (2000)
26. Tsai, A., Yezzi, A., Willsky, A.S.: Curve evolution implementation of the Mumford-Shah functional for image segmentation, denoising, interpolation, and magnification. IEEE Trans. Image Process. **10**(8), 1169–1186 (2001)
27. Vese, L.A., Chan, T.F.: A multiphase level set framework for image segmentation using the Mumford and Shah model. Int. J. Comput. Vis. **50**(3), 271–293 (2002)
28. Vese, L.: Multiphase Object Detection and Image Segmentation. In: Osher, S., Paragios, N. (eds.) Geometric Level Set Methods in Imaging, Vision and Graphics, pp. 175–194. Springer, Heidelberg (2003)
29. Zhao, H.-K., Chan, T., Merriman, B., Osher, S.: Variational level set approach to multiphase motion. J. Comput. Phys. **127**(1), 179–195 (1996)